LABORATORY ANALYSIS OF CO_2 STORAGE IN DEPLETED ORGANIC-RICH SOURCE ROCKS FOR CARBON SEQUESTRATION

A Thesis

by

JESSICA EVELYN XAVIER VIEIRA

Submitted to the Graduate and Professional School of
Texas A&M University
in partial fulfillment of the requirements for the degree of

MASTER OF SCIENCE

Chair of Committee,	I. Yucel Akkutlu
Committee Members,	J.C. Cunha, Mauro Becker
Head of Department,	Akhil Datta-Gupta

May 2022

Major Subject: Petroleum Engineering

ABSTRACT

Carbon capture and sequestration processes can use the infrastructure of unconventional EOR projects targeting organic-rich source rocks and use the existing fluids separation and injection technologies. Accordingly, source rocks, also called shale, have unique petrophysical properties that facilitate the storage of large amounts of gas, such as methane and carbon dioxide, at high pressure. Several laboratory methods have previously been developed to measure the storability of gases such as methane and carbon dioxide (CO_2) in shale. In my thesis, I investigate source rocks for carbon sequestration by applying an existing gas storage method based on Boyle's law. Six shale samples with an average 5% total organic carbon were considered and total (free + sorbed) gas storability is predicted using key laboratory-measured parameters: pore volume, pore compressibility, Langmuir volume, Langmuir pressure, and sorbed phase density. The Santos and Akkutlu (2013) method considered pore volume changes and used a linear form of the Langmuir model to estimate gas storability in the laboratory. Experiments were conducted at 77°F for a pressure range of 1,500-3,200 psi. Four of the samples showed preference for CO_2 storage in the sorbed phase over the compressed free phase indicating that sequestration in source rocks will be dominated by the CO_2 adsorption as the trapping mechanism. The maximum amount stored sorbed volume ranged from 520 to 2,040 scf/ton while the maximum compressed free gas stored ranged from 83 to 460 scf/ton respectively. To maintain the earth's temperature from rising by 2°C by 2050, it has previously been predicted that about 45 giga-tons of CO_2 in total must be sequestered by 2050 considering yearly emission reductions are made. Based on my experimental results I find out that carbon sequestration in North American source rocks should suffice to reach to this target. Barnett shale alone, including in my calculation the total (both developed and not-yet developed)

acreage, has the capacity to store 435 giga-tons of CO_2. The Marcellus shale, on the other hand, is a large storage unit with a carbon sequestration capacity of 1000 gigatons, i.e., 1 tera-ton. I conclude that the source rocks as volumetric storage units have a significant capacity for the carbon sequestration. This is mainly due to the potential of the organic material in source rock to store carbon dioxide in sorbed states.

DEDICATION

To God be the glory.

Dedicated to my grandmother Eli and to my parents Antonio and Veronica.

ACKNOWLEDGEMENTS

I thank my committee members for their contribution to my thesis. I also would like to thank Seungmo Kang for sharing his expertise and data with me.

CONTRIBUTORS AND FUNDING SOURCES

Contributors

This work was supported by a thesis committee consisting of Professors Dr. I. Yucel Akkutlu [advisor] and Dr. J.C. Cunha of the Harold Vance Department of Petroleum Engineering and Professor Dr. Mauro Becker of the Department of Geology and Geophysics.

The data analyzed for Chapter 4 and 6 was provided by Seungmo Kang and was published in 2011 in the Society of Petroleum Engineers Journal.

All other work conducted for the thesis was completed by the student independently.

Funding Sources

Graduate study was supported by Graduate Program Fellowships and the John C. Calhoun, Jt. Fellowship from Texas A&M University and Graduate Fellowship Fellowships from Chevron Corporation.

NOMENCLATURE

B_{gi,CH_4} = Gas formation volume factor for CH_4 gas

B_{gi,CO_2} = Gas formation volume factor for CO_2 gas

C_p = Coefficient of isothermal pore volume compressibility, 1/psi

G_{CH4} = Free gas storage capacity of CH_4 gas, scf

G_{CO2} = Free gas storage capacity of CO_2 gas, scf

G_f = Free gas storage capacity, scf/ton

$G_{f,\,dev}$ = Free gas storage capacity at developed area, scf

G_s = Sorbed-gas storage capacity, scf/ton

G_t = Total gas storage capacity, scf/ton

G_{sL} = Langmuir maximum sorption storage capacity, scf/ton

M = Molar mass, g/mol

n_d = Number of moles of dead volume, mol

n_{df} = Number of moles of dead volume at equilibrium pressure, mol

n_{di} = Number of moles of dead volume at initial pressure, mol

n_r = Number of moles in reference cell, mol

n_{rf} = Number of moles in reference cell at equilibrium pressure, mol

n_{ri} = Number of moles in reference cell at initial pressure, mol

$n_{s,free}$ = Number of free moles stored, mol

$n_{s,s\,i}$ = Number of sorbed moles stored at stage i, mol

$n_{s,s}$ = Number of sorbed moles stored, mol

$n_{s,s\,max}$ = Maximum number of moles stored in sorbed phase, mol

$n_{s,tot}$ = Total moles of gas stored in sample, mol

$n_{s,tot\,i}$ = Total number of moles stored in sample at stage *i*, mol

$n_{s,tot\,f}$ = Total moles of gas stored in sample at equilibrium pressure, mol

P = Pressure, psi

P_{atm} = Absolute atmospheric pressure initially in sample

P_{df} = Final dead volume pressure, psi

P_{di} = Initial dead volume pressure, psi

P_i = Pressure of sample cell at initial pressure, psia

$P_{i,res}$ = Average initial reservoir pressure, psia

P_f = Pressure of sample cell at equilibrium pressure, psia

P_L = Langmuir pressure, psia

P_p = Pore pressure, psia

P_{rf} = Final reference cell pressure, psi

P_{ri} = Initial reference cell pressure, psi

P_{sc} = Pressure at standard conditions, psi

P_1 = Absolute initial reference volume pressure

R = Universal gas constant, psia-ft^3/mol-K

S_{wi} = Initial water saturation, fraction

T = Temperature, °F

T_i = Temperature at initial reservoir conditions, °F

TOC = Total organic carbon

T_{SC} = Temperature at standard conditions, °F

scf = cubic feet of volume of gas measured at standard conditions of 60°F and 14.7 psia

T_f = Absolute temperature of reference volume and sample after P_f is stabilized temperature at equilibrium, °C

T_1 = Absolute temperature of sample pore volume at atmospheric pressure

T_{1r} = Absolute temperature of reference volume at P_1

V_{ads} = Adsorbed gas volume, cc

V_c = Sample chamber volume, cc

V_{Cp} = Volume due to pore compressibility, cc

V_{eff} = Effective pore volume associated with Helium free gas, ft^3

$V_{eff\,1}$ = Effective pore volume associated with CO_2 and CH_4 free gas, ft^3

V_G = System grain volume, cc

V_p = Sample pore volume, cc

V_{pi} = Initial sample pore volume, cc

V_{p0} = True pore volume, ft^3

V_r = Reference cell volume, cc

V_{rf} = Final reference cell volume, cc

V_{ri} = Initial reference cell volume, cc

V_{si} = Initial sample pore volume, cc

V_{sf} = Final sample pore volume, cc

$V_{s,s\,max}$ = Maximum volume of stored sorbed gas, cc

V_v = Valve displacement volume (from open to closed position)

w = Weight of sample, ton

z_{df} = Compressibility factor of dead gas at equilibrium pressure

z_{di} = Compressibility factor of dead gas at initial pressure

z_f = Compressibility factor at final equilibrium pressure

z_{i,CH_4} = Compressibility factor of CH_4 at initial reservoir pressure

z_{i,CO_2} = Compressibility factor of CO_2 at initial reservoir pressure

z_{rf} = Compressibility factor at reference cell at equilibrium conditions

z_{ri} = Compressibility factor at reference cell at initial conditions

z_{P_f} = Compressibility factor at reference cell equilibrium pressure P_f

z_1 = Compressibility factor at P_1 and T_1

GREEK SYMBOLS

$\rho_{s,free}$ = Free-phase density at standard conditions, g/cc

$\rho_{s,s}$ = Sorbed-phase density at standard conditions, g/cc

$\rho_{s,max}$ = Maximum sorbed-phase density at reservoir conditions, mol/cc

ϕ = Porosity, fraction

TABLE OF CONTENTS

Page

LIST OF FIGURES

Page

LIST OF TABLES

Page

1. INTRODUCTION

1.1 Overview

Human activities increase the emission of gases, such as methane (CH_4) and carbon dioxide (CO_2), which are main contributors of the greenhouse effect. They contribute 17% and 74% respectively to the total greenhouse gas emissions (Ritchie and Roser, 2020). This ongoing greenhouse effect has negative consequences at various levels that could have the potential to endanger both nature and humanity. Most importantly, it could accelerate global warming to a scale that the natural course of the earth's climate could change irreversibly. Currently, it is difficult to predict the consequences of a changing climate on life on earth with certainty, but in order to preserve and protect, international climate agreements have been introduced as commitments aimed at reducing emissions.

There is consensus that the current global greenhouse gas emissions far exceed the earth's natural uptake. The earth is capable of naturally absorbing up to 200 megatons per year (Mtpa) of CO_2 (IPCC, 2001) through land and ocean sinks. However, as of 2021, *Our World in Data* reported that an estimated 36,000 Mtpa of CO_2 has been emitted globally (Ritchie and Roser, 2021). According to one estimate, only the energy-related emissions in 2020 was 31,500 Mt (IEA, 2021a). The earth would require more than 150 years to eliminate this large volume. **Figure 1** shows that emissions from fossil fuels have increased exponentially. Interestingly, half of the anthropogenic CO_2 emissions took place in a relatively short period of time, between 1970 and 2010, when a rapid economic and population growth took place (Pachauri, 2014)

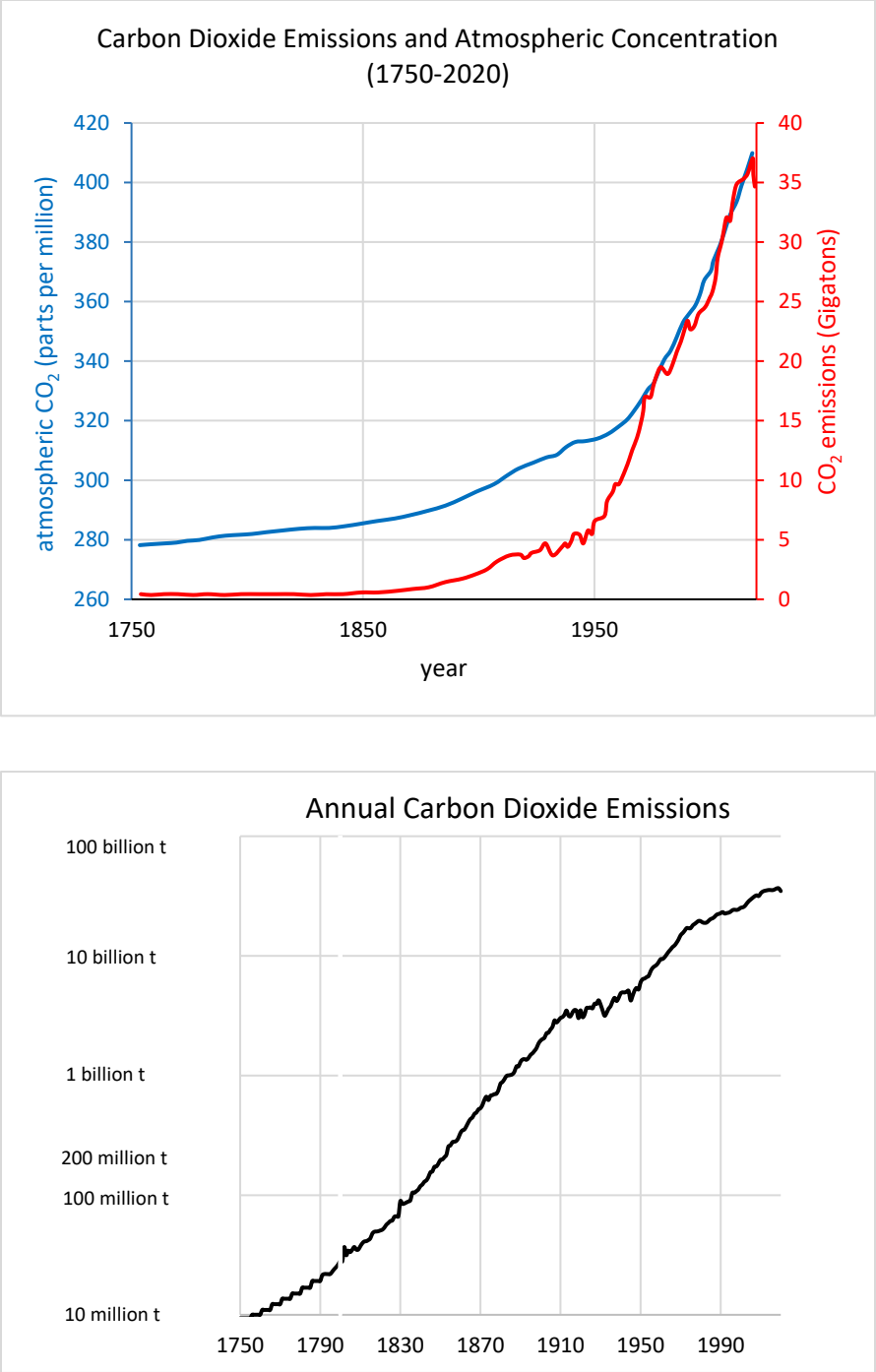

Figure 1. (bottom) Annual CO_2 emissions from burning of fossil fuels and atmospheric concentration during the years 1750-2020. (top) Annual CO_2 emissions in billion tons from burning of fossil fuel edited from Our World in Data. Earth's CO_2 adsorption capacity is

200Mtpa. Figures adapted from Ritchie and Roser (2020) from Our World in Data.**1.2 Greenhouse Gas Emissions Reduction Efforts**

Rapidly increasing emissions are currently enforcing countries to develop ambitious plans for the reduction of their individual CO_2 emissions. However, this is an arduous task, in particular for developing countries with significant volumes of emission. The current global CO_2 capture capacity is 40 Mtpa (CCS Institute 2020, IEA 2021a). As such, CO_2 emissions have been far exceeding the efforts for its reduction. The IEA net zero report (IEA, 2021b) estimates that 1,600 Mtpa capture is required by 2050 to limit global temperature increase to 2°C assuming yearly emissions decrease occur until 2050. *Our World in Data* emphasizes that global emissions have not yet peaked (Ritchie and Roser, 2020), therefore, it is anticipated that the emissions will continue to increase significantly and that the efforts to control emissions at large scale should begin without further delay. The longer these efforts are delayed, the higher the greenhouse gas capacity ceiling requirement will be (Zahasky and Krevor 2020). Due to its urgency, scientists and engineers have been and continue to actively seek solutions to retard and control the rise of greenhouse gas emissions.

The prevalent proposed solution to mitigate the emissions is to implement renewable energy and electric vehicles (EVs) to replace fossil fuels. However, this will require upscaling of various industries with significant emissions. Azadi et al. (2020) estimate that nearly 10% of the total global energy-related emissions in 2018 stemmed from minerals and metal production. Recent publications highlight the negative environmental and social impacts of activities such as steel and cement production (Xu et al. 2020, Azadi et al. 2020, Wang et al. 2020, Nature Editorial 2021). Mining activities necessary for large-scale development of the battery industry include long-distance transportation, electrical equipment usage, mineral refining, and material processing

which is a particularly energy intensive process. An important factor that is likely to increase the mining carbon footprint is decreasing ore grade. As the ore quality decreases, larger volume of the raw mineral is needed to produce the equivalent amount of mineral, resulting in a further increase in the onsite mining activities (Azadi et al. 2020). Presuming these scenarios extend to other minerals, renewable energy and EVs may not provide the necessary emissions reduction foreseen.

1.3 Carbon Sequestration as Greenhouse Gas Emission Control

Thus, carbon capture, utilization and sequestration has become key to mitigate greenhouse gas emissions. As mentioned earlier, CO_2 sequestration could be achieved by the combined integration of plants, soils, and the ocean. One approach is then to increase the rate of sequestration through changes in forestry, land use or in direct capture and injection into the ocean. Another approach is to directly capture and store the gases in subsurface storage units that have reliable seals, i.e., geological sequestration.

Zahasky and Krevor (2020) estimate that there exists 10 million Mt of prospective geological storage sites available. They further argue that 2.7 million Mt of carbon sequestration is required by 2050, which requires roughly 27% of the geological storage sites used for CO_2 injection and storage. This indicates that geological storage is physically possible to achieve the set targets. Therefore, geological sequestration is considered as a method with potential for large (megatons) scale sequestration.

Geological sequestration efforts have so far focused on aquifers and depleted conventional reservoirs, in particular in countries with governments that allow carbon credit as a permit to emit a fixed amount of CO_2 to the atmosphere. Successful projects include deep saline aquifers and offshore petroleum reservoirs in Norway and Canada. Since there is significant interest in

subsurface sequestration, the introduction of source rocks (such as depleted shale wells) becomes relevant as they offer potential alternative sites for sequestration. By repurposing existing infrastructure and applying the improved recovery concepts, Occidental Petroleum is already performing carbon sequestration in its Permian Basin assets, currently storing 20 Mtpa (United Nations, 2019). This effort creates a synergy with CO_2-enhanced shale oil recovery. During an average EOR process roughly 40% of the injected CO_2 stays in the reservoir and sequestered; whereas the produced CO_2 can be separated and injected back. If this process can be applied to other major shale plays in the United States, such as the Eagle Ford and Bakken, the carbon sequestration in shale rocks can have a major impact. The knowledge gained through experience in carbon sequestering in source rocks could be extended to other shale oil/gas producing fields located in Canada, Argentina and China.

In this study, I will focus on shale gas formations. Previously developed, depleted, and fractured shale gas formations are promising alternative storage locations for several reasons. Firstly, these formations have been effectively holding a large volume of greenhouse gas (methane) for thousands of years -- why not inject another greenhouse gas CO_2 for sequestration? The infrastructure to store, transport and inject the gas already exists. Thousands of vertical and horizontal wells have already been drilled and completed, hence the target formations for sequestration are easily accessible. Because the region of interest has already been developed for production, pipelines have already been built to transport the gas to market. Hence, an entire network is already in place that can be repurposed for the delivery and injection of CO_2 into the desired subsurface formation (**Fig. 2**). For example, Sminchak et al., 2012 investigated the infrastructure requirements for large-scale CO_2 storage applications in midwestern United States. Additionally, major cities near source rocks (such as Dallas/Fort Worth near Barnett; New York

City, Pittsburgh, Columbus near Marcellus) can benefit by creating a CO_2 capture and storage system for the city's high emission points such as power plants, cement factories etc. CO_2 would be transported from the source through the existing pipelines to the well head.

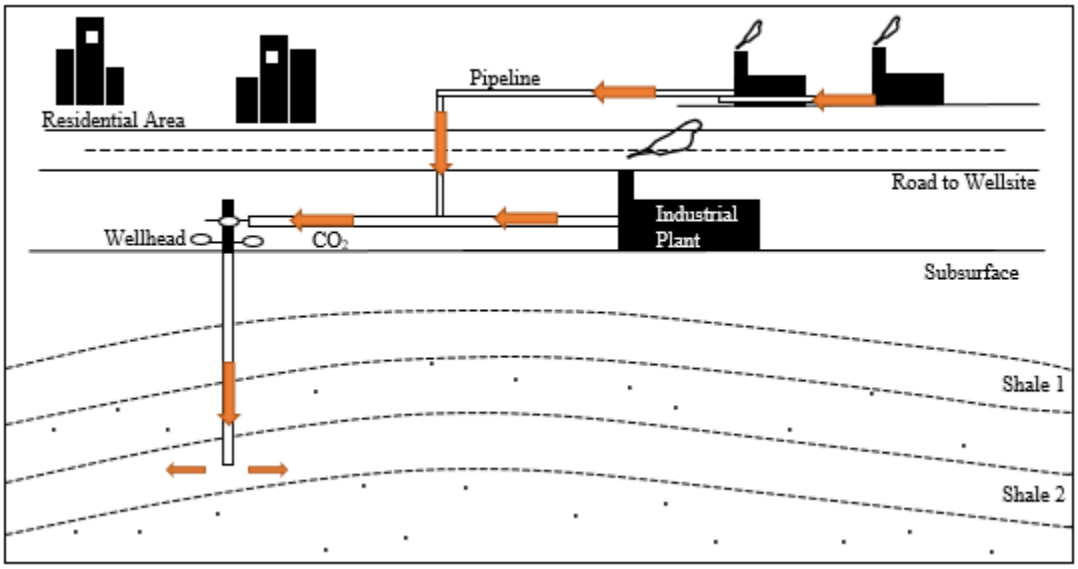

Figure 2 — Visual representation of existing infrastructure in an industrial setting transporting CO_2 to storage site from the source.

1.4 Carbon Sequestration Potential in North America

The upstream petroleum industry possesses not only the infrastructure needed but also the key knowledge necessary to design the carbon sequestration operations targeting the source rocks. Storability measurement of geological formations has been important for estimation of *in situ* oil, water and gas volumes. These measurements have been part of the effort to assess the economic potential of the conventional oil and gas resources. Similarly, storability measurement is also important in identifying a rock's quality for carbon sequestration location. However, our understanding of the storage capacity of the unconventional resources such as the source rocks for

preliminary calculations of sequestration volumes is at its infancy. New and reliable technologies such as downhole tools and laboratory methods are critical for the sequestration considerations in source rocks. In this thesis, I discuss laboratory methods available, new concepts and trends observed in estimating the gas storage capacity of source rocks. A new methodology will be introduced in order to estimate the greenhouse gases (CH_4, CO_2) storage capacity of shale samples.

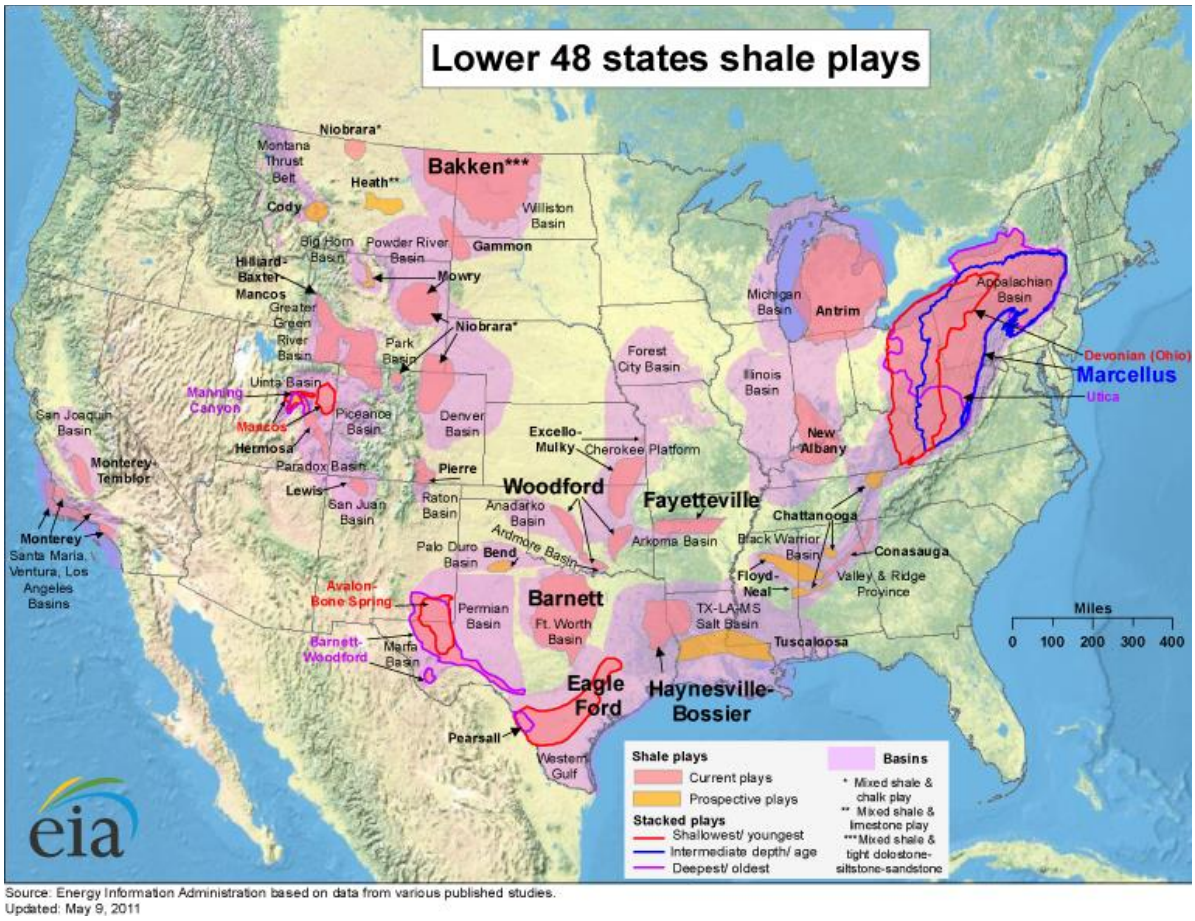

Figure 3 — Map of shale plays in the United States reprinted from EIA (2011).

A map of showing the locations of gas shale plays in the US is presented in **Fig. 3**. The focus would be on Barnett, Marcellus and Fayetteville gas shales. Original gas in-place in these formations has already been calculated assuming the stored fluid is pure methane. (This assumption is reasonable for shale gas.) **Table 1** shows the estimated values taken from Svetlana

et al. (2018). Remember that these calculations have large uncertainties due to geological, geochemical, and petrophysical variability in these formations. Also, the uncertainties further increase due to lack of data. Despite these uncertainties, it is interesting to note the significant difference in storing gas in the Marcellus due to the large acreage the formation holds. The latter stores nearly 25 times more natural gas than that in Fayetteville and about 3.6 times more than that in Barnett.

Table 1 — Original Gas in Place for Source Rocks adapted from Svetlana et al. (2018).

Parameter (unit)	**Barnett**	**Marcellus**	**Fayetteville**	**Haynesville**
Initial Pressure (psi)	3,000	3,500	2,000	10,000
Temperature (°F)	190	135	223	315
z-factor for CH_4	0.8343	0.8595	0.8288	1.4764
z-factor for CO_2	0.4011	0.4583	0.2835	1.1436
Gas in-Place (Tscf)	508	1,813	75	700

Let us focus to Barnett shale with an estimated 508 Tscf of natural gas in-place, but keep in mind that the same discussion I will follow can be extended to the others. The question one needs to ask is the following: If I consider CO_2 sequestration in the same source rock under the same initial pressure and temperature conditions, would the amount of CO_2 stored be the same? (I consider the storage estimations made using the initial reservoir pressure of each site, because this is the highest pressure that I can consider carbon sequestration without compromising the sealing capacity of the rock.) The answer to my question is no; because, even though CO_2 is going to take up the same pore volume in the rock at the same pressure and temperature as methane did, these molecules behave differently. More precisely, they maintain different qualities such as density and formation volume factor. In essence, maintaining the same pressure and temperature, when forced into a tank, these gases will be compressed at a different level. In turn, when we apply the

volumetric method, the calculated gas in-place will change. Allow me to explain my point using numbers.

In Svetlana et al. (2018) the natural gas in-place in a shale play is calculated using the volumetric equation:

$$G_{CH_4} = \frac{Ah\,\phi\,(1-S_{wi})}{B_{gi,CH_4}} \quad \text{.....(1)}$$

Table 2— Formation parameters and their volumetric equation constant numerator values.

	Average Total Formation Area (ft^2)	Average Formation Thickness (ft)	Porosity (ϕ)	Initial Water Saturation (Sw_i)	Constant
Barnett	3.987E+11	300	0.060	0.25	5.382E+12
Marcellus	2.286E+12	125	0.019	0.30	3.801E+12
Fayetteville	1.199E+11	200	0.050	0.25	8.991E+11
Eagle Ford	5.576E+09	200	0.035	0.20	3.123E+10
Haynesville	1.818E+11	250	0.1023	0.318	3.17156E+12

In Equation (1) the acreage A, formation thickness h and water saturation S_{wi} are all fixed quantities regardless of the nature of the gas being considered for storage. Only the formation volume factor B_{gi} changes with the type of gas because, as shown in **Eq. 2**, it depends on z_{i,CH_4} the corresponding compressibility for CH_4 at the initial reservoir pressure (P_i) and initial reservoir temperature (T).

$$B_{gi,CH_4} = \frac{P_{sc}}{zT_{sc}} \frac{z_{i,CH4}\,T}{P_i} \quad \text{.....(2)}$$

The amount of CO_2 that could be stored at initial reservoir conditions can be estimated by substituting B_{gi,CO_2} into **Eq. 1**, where the compressibility factor for CO_2 is z_{i,CO_2} needs to reflect the change in the stored fluid. Taking the numerator of **Eq. 1** as constant, the amount of original gas in place (OGIP) is proportional to the inverse of the gas formation volume factor. Tabulated values of the constant value for different formations are shown in **Table 2**.

$$G_{CH_4} = \frac{const.}{B_{gi,CH_4}}$$

$$G_{CO_2} = \frac{const.}{B_{gi,CO_2}}$$

Therefore, to convert OGIP from CH_4 to CO_2, the following relationship is used:

$$G_{CO_2} = G_{CH_4}\left(\frac{B_{gi,CH_4}}{B_{gi,CO_2}}\right) \quad \text{.....(3)}$$

Let us take the initial reservoir pressure P_i for Barnett shale is 3000 psi. This gives the following formation volume factor values for methane and CO_2:

$$B_{gi,CH_4} = \frac{P_{sc}}{zT_{sc}}\frac{z_{i,CH4}\,T_i}{P_{i,res}} = 0.02819\,\frac{0.8343\ x\ 649.67\ °R}{3000} = 5.093x10^{-3}$$

$$B_{gi,CO_2} = \frac{P_{sc}}{zT_{sc}}\frac{z_{i,CH4}\,T_i}{P_{i,res}} = 0.02819\,\frac{0.4011\ x\ 649.67°\mathrm{R}}{3000\ psi} = 2.449x10^{-3}$$

Table 3 — Calculated CO_2 volume at initial conditions from Svetlana et al. (2018) methane volume values using the inverse relationship of gas stored and $\boldsymbol{B_{gi}}$.

	Barnett	**Marcellus**	**Fayetteville**	**Haynesville**
Original Gas (CH_4) in-Place (Tscf)	508	1,813	75	700
Volume of CO_2 to be sequestered (Tscf)	1,057	3,400	219	904

Substituting these values into Eq. 3, we obtain the amount of CO_2 that can be stored in Barnett:

$$G_{CO_2} = 508\,Tscf\left(\frac{0.0050932}{0.0024486}\right) = 1056.7\,Tscf \quad (4)$$

This value (as well as the values for carbon sequestration in Marcellus, Fayetteville, and Haynesville are tabulated in **Table 3.** Clearly, the amount of sequestered gas in terms of Tscf is increased by a factor of 2. This shows the intricacies in carbon sequestration.

If we consider the stored amount in terms of tons of gas, the calculated volume must be multiplied by the gas density. Barnett can hold 55.1 gigatons of carbon dioxide, Marcellus 177.4 gigatons, Fayetteville 5.5 gigatons, and Haynesville 47.8 gigatons. Together these four source rocks would hold 291 gigatons of CO_2.

I would like to reiterate that the estimated numbers have large uncertainties. In addition, when we consider carbon sequestration in source rocks, the storage based on the classical volumetric method has an added complexity that I intend to delve into in my thesis in the following pages. The source rocks storing gases have the ability to store gas in different thermodynamic states, namely, free gas, adsorbed gas and absorbed (dissolved) gas. The calculation shown in the previous pages consider only the free gas occurrence in the source rock, G_{free,CO_2}. Because it does not count the stored sorbed amount (G_{s,CO_2}), the estimate is a rather low. In this thesis, I will show that the

source rocks can store gases significantly more due to sorption, and because sorption of CO_2 is larger than CH_4, the increase could be much higher than one could estimate intuitively.

Consequently, the total CO_2 storage capacity of a shale play has free and sorbed gas components:

$$G_{total} = G_{free,CO_2} + G_{s,CO_2} \quad \text{.....(5)}$$

From a natural gas production point of view, the contribution of the sorbed gas to the reserve could be considered insignificant, but from carbon sequestration point of view, it is important. In fact, as I will show in my thesis, the sequestered amount in the form of sorbed gas is much more significant than the free gas amount.

2. GAS STORAGE CONSIDERATIONS IN SOURCE ROCKS

Prior to the interest in production from shale formations, storage capacity measurements were performed in other types of geological formations such as the conventional ones (sandstones and carbonate rocks) and coalbeds. It is widely recognized that conventional rock samples store fluids volumetrically when the interconnected pore-network volume of rock behaves as the storage unit. Under the subsurface conditions, the larger the pore pressure is maintained, the larger volume of fluid is stored in the unit as a compressed fluid. Compressibility equation of state tells us accurately the amount of gas that can be sequestered in an effective pore volume V_p at pore pressure P, and formation temperature T. In number of moles n, the amount of gas stored is: $n = PV_p/(zRT)$.

However, storage in source rocks such as coalbed and organic-rich shale are different. In the 1980s, it was found that the main storage mechanism in coal seams was adsorption (Gray, 1987; Mavor et al., 1990). In the early 2000s, there were many experimental and theoretical studies on the sorption capacity of coals not only using methane, but also CO_2 (Krooss et al. 2002, Siemons and Busch 2007, Li et al. 2010). The goal of these investigations were coalbed methane production and CO_2-enhanced coalbed methane production. More recently, with increasing interest in shale gas production, storage capacity of shale formations was also measured and analyzed. These analyses of shale gas formations are insightful also for the sequestration considerations.

2.1 Langmuir Isotherm

Adsorption has been predominantly measured by the Langmuir model. Langmuir's isotherm relates pressure and stored gas capacity by calculating the number of molecules adsorbed onto a surface in a single layer (**Eq. 6**). The isotherm is composed of two fundamental parameters called

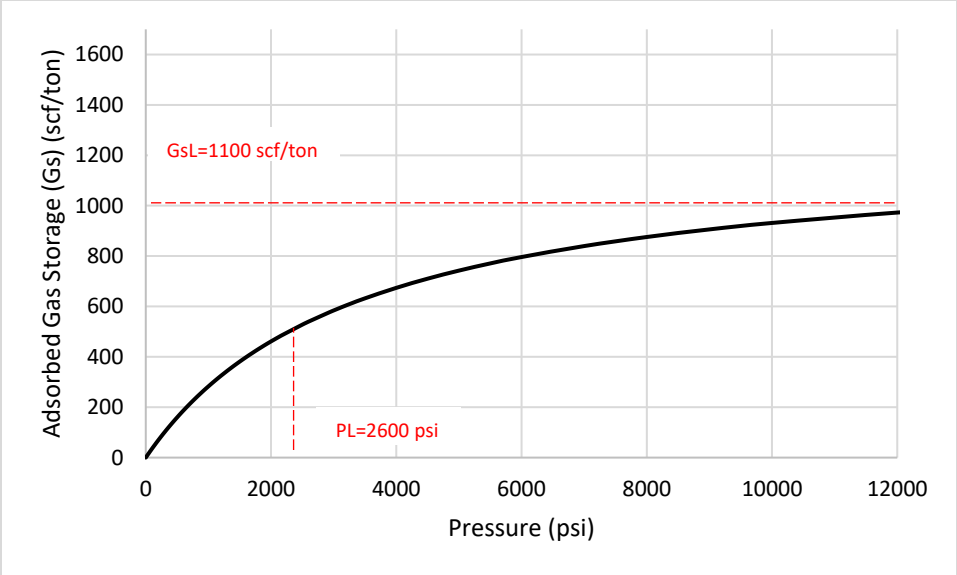

Figure 4 — Langmuir isotherm example highlighting how the Langmuir pressure and Langmuir volume parameters are attained.

Langmuir pressure (P_L) and Langmuir volume in terms of scf/ton (G_{sL}). Langmuir volume is the volume obtained once the isotherm is level, while the Langmuir pressure is the corresponding pressure at the half value of the Langmuir volume (**Fig. 4**).

$$G_s = G_{sL}\frac{P}{P+P_L} \quad \text{.....(6)}$$

2.2 Shale Petrophysical Properties

Most of the shale gas formations are rich in organic matter, also known as kerogen. Total organic carbon (TOC) is commonly used as a proxy for the organic matter present in the rock (Dembicki, 2017). Kerogen is critical component of the source rock, because it indicates the generation potential of hydrocarbons. Thermal maturity characterizes the extent which kerogen has been transformed to hydrocarbons due to increasing burial depth and temperature. When

thermal maturity increases, kerogen porosity also increases as new pores form from the expulsion of generated hydrocarbons in the rock. Thus, high maturity rocks with high TOC provide the largest volume of organic pores and the highest initial gas in place capacity.

From the gas storage point of view, kerogen with its organic nanopores can be considered analogous to coal. Hence, shales with their organic and inorganic pore networks are a dual storage medium that allows volumetric storage (mainly in the inorganic part), as well as sorption storage (mainly in the organic part) (Kang et al., 2011). However, unlike coalbeds, shale gas formations as source rocks could be significantly over-pressured. This excessive pore pressure leads to development of organic nanopores that are not only suitable for sorption but also volumetric -highly-compressed- gas storage.

Key petrophysical characteristics of shale are porosity, saturations, permeability, and total organic carbon (TOC). Each of these affect the long-term total gas storability of the rock. Ultra-low shale permeability and anisotropy, for example, limit vertical migration of the stored fluid within the formation and provides a natural seal. These formations are quite thick and they held natural gas for centuries; they can indeed store greenhouse gases, too. Organic porosity enables storage of large amounts of CO_2 in adsorbed and dissolved (absorbed) states in kerogen due to strong molecular interaction forces between CO_2 and the organic pore walls (Kang et al. 2011; Kang et al.2014; Kim et al. 2019). These pores are in the micro- to nano-meter range and they are prolific within the organic material (Ambrose et al. 2010, Wang and Reed 2009). The number of organic pores present in the rock and the pore size distribution are controlled by the thermal maturity and TOC of the rock: the higher the TOC and maturity, the more organic pores the rock sample has (Busch et al. 2008, Nuttall et al. 2005, Lu et al., 1995). Sorption of CO_2 is amplified

due to molecular polarity of CO_2; the dipole moment of CO_2 is known to be much higher than the other naturally-occurring gases such as nitrogen and methane.

In addition, steric effects also lead to high CO_2 adsorption. Linear CO_2 molecular structure facilitates access to minute pores (Kang et al., 2011, Charoensuppanimit et al. 2016). Linearity also promotes closer packing of the sorbed CO_2 molecules. In this article the authors consider the mechanisms of sorption not only as the means of storing fluids such as CO_2 but also as a highly effective trapping mechanism for carbon sequestration. Hence, it is through the trapping effect of sorption mechanisms that considerable carbon sequestration is possible in organic-rich

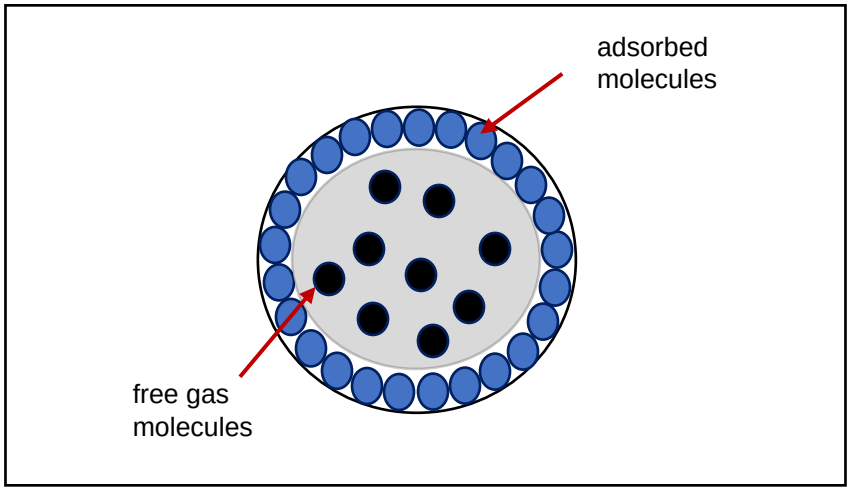

Figure 5 — Schematic showing free and adsorbed gas in the pore

shale formations (**Fig. 5**). Thus, the petrophysical components of the shale are important and must be carefully considered from sealing and trapping points of view.

3. LABORATORY METHODS FOR SEQUESTRATION CAPACITY IN GEOLOGICAL FORMATIONS

3.1 Previous Laboratory Studies of CO_2 and CH_4 Storage

Different studies considered different parameter effects on shale gas storage and they mostly employed the volumetric method. Nuttal et al. (2005) studied Devonian black shale samples in Kentucky for enhanced natural gas production potential of CO_2 injection. They concluded that total organic carbon (TOC) can be used as a proxy for adsorption capacity in shale due to their direct and linear relationship. They constructed Langmuir isotherms for the prediction of the mono-layer adsorption based on a method proposed by Mavor (1990). Alternatively, authors like Busch et al. (2008) calculated sorption volumes using the BET model (Brunuer et al., 1938) which considers multi-layer adsorption. Zhang et al. (2012) stated that TOC is the primary control on gas adsorption in shale gas systems. Their study included methane gas experiments and thermal maturation considerations, which concluded that thermal maturity mostly affects adsorption capacity at low pressures. Heller and Zoback (2014) performed CO_2 and CH_4 adsorption measurements on mineral surfaces and gas shale samples. They determined that although TOC is the main determinant of adsorptive capacity of a sample, in the small TOC limit, clays that make up the shale sample such as illite and kaolinite are also responsible for significant gas storage. Additionally, the authors argued that swelling of the organic material could potentially affect adsorption (Lin et al. 2007, Hol et al. 2011). Tan et al. (2014) concluded that thermal maturity increases the sorption capacity and moisture decreases it as water molecules compete to occupy the adsorption sites.

3.2 Sorption Considerations

Sorption includes both adsorption and absorption. Adsorption is the adherence of gas molecules to the exposed surface area of the rock's pore network. The surface area refers to the internal surfaces of the walls of the pores, pore throats, and fractures. Adsorption occurs primarily in the organic pores due to the affinity of the organic material with the CO_2 molecule and the large surface area its pores embody (Kang et al. 2011). Absorption, on the other hand, is the dissolution and retention of gas molecules by the residual liquids (oil, condensate, and water) or by the organic material and solid minerals composing the inorganic matrix. Here, it should be mentioned that no laboratory method currently exists which measures adsorbed and absorbed gas volumes separately. Instead, there are methods that measure the total sorbed gas.

The total gas storage in an organic-rich shale is the summation of the sorbed and free gas components. It is important to note that the free gas storage is controlled by the pore pressure and temperature of the shale formation, in particular the pressure. Because CO_2 is a relatively compressible fluid, the higher the reservoir pressure is maintained during the storage, the more compressed gas can be stored in the reservoir. Similarly, the sorption mechanisms are directly dependent on the pressure. Hence, it is ideal to store CO_2 in shales at high pore pressure. However, it should be noted that the pressure should not be higher than the initial formation pore pressure, because over-pressuring the formation beyond its natural strain limits could lead to new deformations, resulting in formation of new fractures, faults and fissures, or activation of the healed fractures, which are obviously not desired for the long-term storage of CO_2. The currently exploited shale formations for natural gas production are over-pressured formations. Hence, high-pressure carbon sequestration in organic- rich shale rock could supply a significant portion of CO_2 storage capacity in North America.

3.3 Prevalent Laboratory Methods

Three main laboratory techniques are used to measure gas storability of a rock: volumetric, gravimetric, and chromatographic. The two most common methods employed in reservoir petrophysics laboratories are the volumetric and gravimetric methods. due to the simplicity of the apparatus and its ability to make rapid measurements. They are described below.

3.3.1 Volumetric Method

The volumetric method is originally employed to pore volume and porosity measurements; therefore, the procedure is the first described for the purpose of investigating pore volume, then for storage in shale samples. The Boyle's Law Double-Cell apparatus (**Fig. 6**) from API RP 40 (1988) is the standard setup. The apparatus is composed of two chambers: Sample and Reference Chambers of known volumes separated by a valve. For accuracy, the Reference Chamber volume V_r and the Sample Chamber volume V_c are calibrated and recorded. V_v consists of the minute voidage associated with the valves' displacement from closed to open position during the measurements. Initially, a dry core sample (consolidated or unconsolidated) is placed inside the Sample Chamber. All the chambers are flushed with Helium gas at low pressure (P_{atm}), then the valves are closed. Valve 1 is opened and the Reference Chamber is filled with Helium gas to a predetermined pressure (P_1), such as 100 psi, from the gas cylinder. The Helium gas is then vented into the Sample Chamber by closing Valve 1 first and opening Valve 2. Sufficient time should be given to the system for helium gas to expand into the Sample Chamber and for the Helium molecules to penetrate into the sample pore network until equilibrium is reached. Pressure measured by the transducer should be stabilized to a constant final value P_f under the equilibrium.

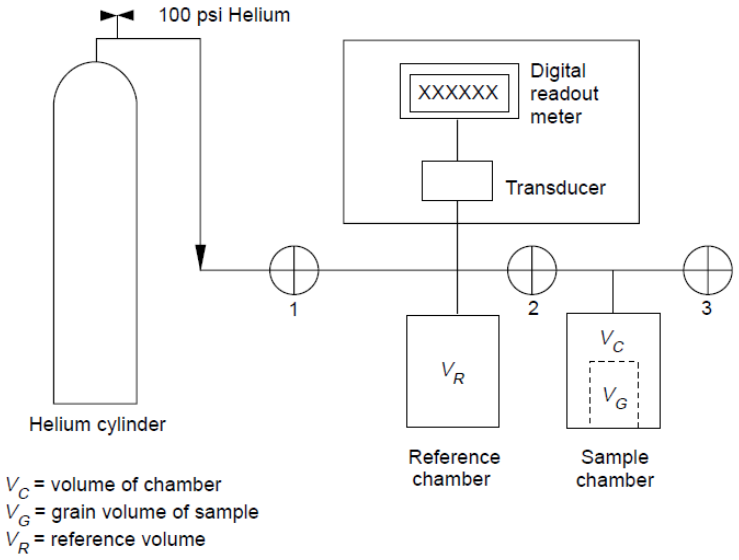

Figure 6 — Double-Cell Boyle's Law Porosimeter reprinted from API RP 40 (1988).

Finally, pore volume is calculated using a Helium mass balance considering the Helium gas in the Reference Chamber V_r, Sample Chamber V_c valves volume (V_v) and sample pore volume (V_p) shown in **Eq. 7** (API RP 40, 1988). The mass balance is actually an equation of conservation of mass stating that the total number moles of Helium is conserved within the apparatus all the time. In other words, the total number of moles of Helium in the chambers prior to its expansion should be equal to the total number of moles of Helium once the equilibrium pressure has been reached.

$$\frac{P_1 V_r}{z_1 T_{1r}} + \frac{P_{atm}(V_c - V_G)}{Z_{atm} T_1} = \frac{P_f(V_r + V_c - V_G + V_v)}{Z_f T_f} \quad \text{(7)}$$

Here V_G is the Grain (or solid) Volume of the rock sample in the Sample Chamber. The mass balance given in **Eq. 7** assumes that no helium is lost or added to the system. This is a reasonable assumption, because the Helium is an inert gas and the experiments are carried at relatively low pressure such that gas leakage during the experiments is negligible. It is further assumed that the

temperature stays constant, i.e., isothermal conditions prevail. Solving **Eq. 7** for void volume and re-arranging, the Grain Volume of the rock sample is determined using **Eq. 8**:

$$V_G = \mathrm{V_c} - \frac{V_r(P_1 - P_f) + V_v P_f}{P_f - P_{atm}} \quad \text{..... (8)}$$

The bulk volume of the sample is measured independently, by directly measuring the dimensions of the sample or using the Archimedes principle. Finally, the pore volume V_p and porosity ϕ are calculated.

The volumetric method for sorption measurements is derived from this API approach. In this study, a similar equipment is used, but the procedure now involves a measurement gas that adsorbs and is used for multiple stages of gas expansion. The reason for multiple-stages is that sorption is highly sensitive to pore pressure: the dependence is nonlinear and the increase in sorbed amount continues monotonously with pressure until the maximum sorption capacity of the rock is reached and until the sorbed amount finally becomes independent of the pressure, which could be in the order of thousand psi. Capturing this dependency in the laboratory is a time-consuming and challenging task but necessary for the sequestration.

Because the reservoir pressure and temperature for CO_2 storage is high, it is important that, once the pore volume of the rock is determined using Helium as the measurement gas, the sorption measurements should proceed with CO_2 at high pressure and temperature conditions. Hence, the two-chamber apparatus is heated to a predetermined (reservoir) temperature using an oil (or water) bath or by keeping the apparatus in an environmental chamber. Following the measurement with Helium gas, the CO_2 sorption measurements should be made at multiple gas expansion stages, allowing the system to reach its final equilibrium pressure value at each stage. At each stage, a new sorbed gas amount is estimated using a new mass balance written for CO_2 in the presence of

sorption as a storage mechanism. This process is repeated at higher pressures until the maximum sorbed gas amount is reached and a sorption isotherm showing the sorbed gas amount as a function of pressure is outlined. This function is strongly nonlinear and as such the measured data points are fit to an adsorption model such as Langmuir model (exhibited in **Fig. 3**) or BET model. The Langmuir (1932) adsorption model, although most suited for low-pressure mono-layer adsorption, is commonly employed in the petrophysics laboratory due to its simplicity and reasonable approximation of the excess sorption (Weniger et al. 2010, Tan et al. 2014).

3.3.2 Gravimetric Method

In the gravimetric method, the same apparatus is utilized and the same steps of obtaining the initial pore volume using Helium gas, followed by CO_2 or CH_4 for storage capacity measurements are applied. However, this method directly measures change in sample mass after the gas volume expansion once equilibrium pressure is reached. The change in mass indicates the amount of gas adsorbed by the sample. Recently, Wu et al (2019) and Du et al (2020) utilized the gravimetric method to measure CO_2 and CH_4 gasses on shale (**Fig. 7**).

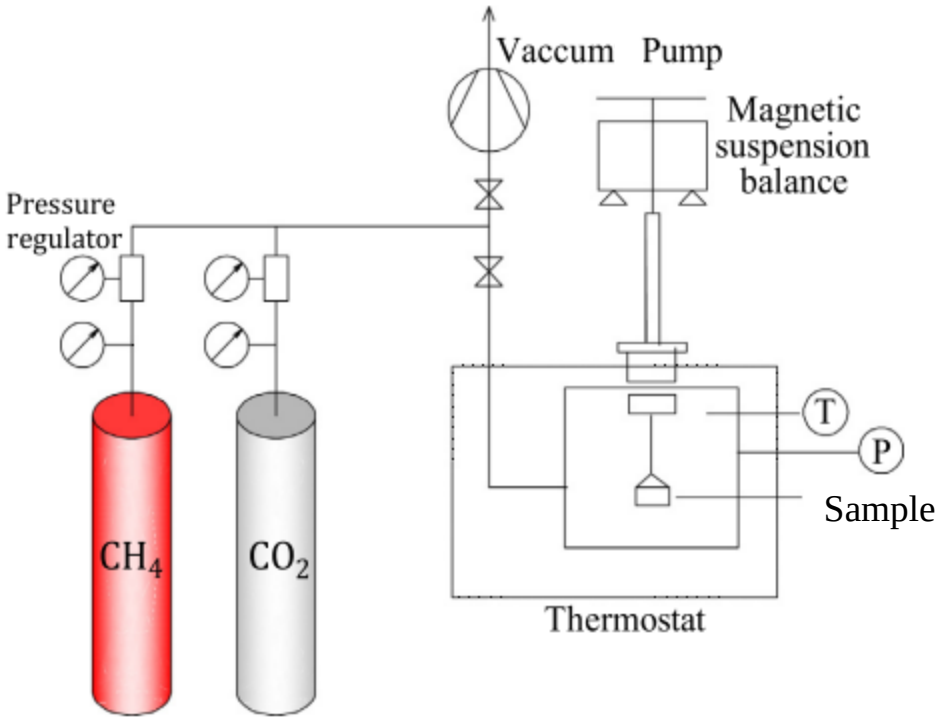

Figure 7 — Schematic diagram of gravimetric experiment set up reprinted Du et al. (2020).

4. LABORATORY PROCEDURE FOR CARBON SEQUESTRATION IN SOURCE ROCKS

The volumetric approach for sorption has been applied to various coal samples in the 1980s as part of the effort to predict the gas storage capacity of coalbed methane formations. Kang et al. (2011) argued that, during isothermal measurements, not only the amount of sorbed gas but also the pore volume available for compressed free gas storage could change in a complex fashion with pore pressure. They attributed these changes in pore volume to two important physical effects. During the CO_2 injection into the source rock, with the increasing pressure, pore volume of the rock sample is expected to change due to:

- Pore volume compressibility of the rock sample
- Sorbed phase effect.

These effects are shown in **Fig. 8**. The first effect is widely known in the petroleum industry and it has previously been shown in various geomechanical laboratories. However, it is not possible to capture this effect using the existing API RP40 setup in the reservoir petrophysics laboratory. Kang et al (2011) proposed changing the Sample Chamber with a Hassler core holder to avoid this problem. The sample is kept under net stress during the gas expansion so that the pore volume is adjusted to the subsurface conditions. Using the volumetric method with the core holder, Kang et al. showed that source rocks such as the Barnett shale could have a dynamically changing pore volume due to the compressibility effect. Later on, Akkutlu and Aldana (2021) extended this work to predict free gas storage under effective stress, when the latter includes an adjustment to the applied stress based on the Biot's coefficient of the sample. The second effect has been introduced by Kang et al. (2011), where the authors argue that organic-rich source rocks, such as

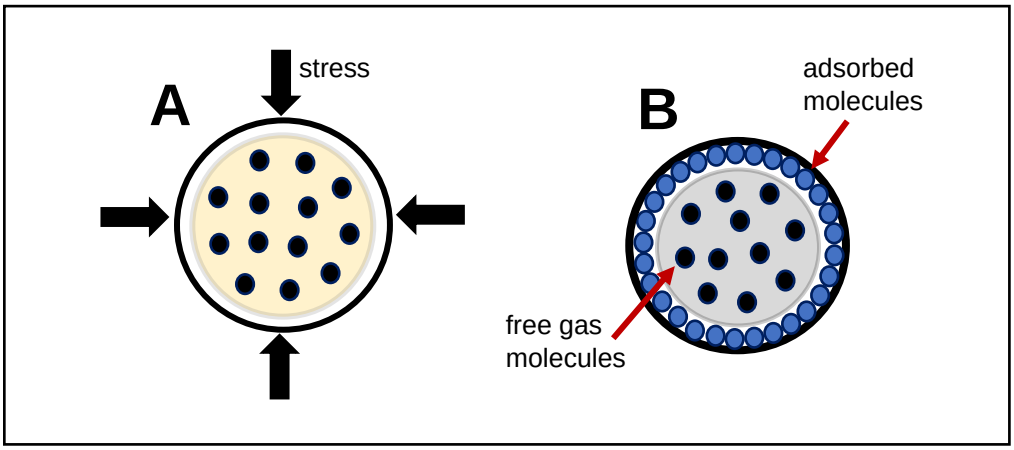

Figure 8— Schematic of change in pore volume occupied by gas molecules. A. Diagram showing volume change due to pore volume compressibility effect. B. Diagram showing volume change due to sorbed phase effect. The effective pore volume in source rock available for gas storage is shown as a gray zone.

shale, have small pore volume and the pore space taken by the sorbed gas molecules (adsorption layer) may cause a noticeable --and in times significant-- reduction in the pore volume. In turn, this leads to a reduction in the storable free gas amount, in particular, in high TOC formations. Therefore, any laboratory investigation on carbon sequestration in source rocks such as organic-rich shale should consider these two effects. Ambrose et al. (2011) proposed a new equation for volumetric gas in-place calculations specifically derived for organic-rich shale gas formations considering these effects in the reservoir during initial gas in-place calculations.

In the laboratory, Kang et al. (2011) proposed a new material balance for the analysis of the free and sorbed gases in the presence of these effects. Their model contains five storage-related parameters whose values should be obtained simultaneously using at least five stages of gas expansion. The authors argued that the measurements and nonlinear curve fitting could have

significant error in the analysis. Santos and Akkutlu (2013) used the same apparatus proposed by Kang et al. (2011) (API RP 40 with a Hassler core holder), but proposed a two-step approach to the measurements in order to reduce the uncertainties raised by Kang et al. (2011). The two-step approach is presented next. Briefly, the first step is for the measurement of the free gas amount, whereas the second is for the sorbed gas amount.

4.1 Estimation of Free Gas Storage Parameters using Helium

The first step involves estimation of only two parameters --out of the original five-- identified by Kang et al. (2011). These two parameters are Pore Volume and Pore Compressibility associated with free gas storage. Helium is used as the measurement fluid during this step. A mass balance equation is used, which includes the two unknown parameters, namely, pore volume at reference pressure (V_{p0}), and the coefficient of isothermal pore compressibility (C_p). To obtain the two unknowns, two consecutive stages of Helium gas expansion are performed.

The initial measurement is separated into dead and sample pore volumes (V_d, V_s) within the sample chamber and reference chamber using a reference temperature of 77°F.

Before gas expansion:

$$n_{ri} = \frac{V_{ri}P_i}{z_{ri}RT} \quad \text{.....(8)}$$

$$n_{di} = \frac{V_{di}P_i}{z_{di}RT} \quad \text{.....(9)}$$

$$n_{s,tot\,i} = \frac{V_{pi}P_i}{z_{P_i}RT} \quad \text{.....(10)}$$

After gas expansion:

$$n_{rf} = \frac{V_{rf}P_f}{z_{rf}RT} \quad \text{.....(11)}$$

$$n_{df} = \frac{V_{df}P_f}{z_{df}RT} \quad \text{.....(12)}$$

$$n_{s,tot\,f} = \frac{V_{sf}P_f}{z_f RT} \quad \text{.....(13)}$$

Altogether, the equation expressing the change in the number of moles stored is presented as **Eq. 14**. Considering the conservation of mass and the application of mass balance, there should be no change in the total volume within the system, such that the total number of moles remains the same at the end of the pressure step.

$$\Delta n_r + \Delta n_d + \Delta n_{s,tot} = 0 \quad \text{.....(14)}$$

The equation is re-arranged by separating the amount of gas stored in the sample.

$$-\Delta n_{s,tot} = \Delta n_r + \Delta n_d = 0 \quad \text{.....(15)}$$

It is also expressed in terms of pressure and volume.

$$\frac{P_i V_{si}}{z_{P_i}} - \frac{P_f V_{sf}}{z_{P_f}} = \frac{P_{rf} V_r}{z_{rf}} - \frac{P_{ri} V_{ri}}{z_{ri}} + \frac{P_{df} V_{df}}{z_{df}} - \frac{P_{di} V_{di}}{z_{di}} \quad \text{.....(16)}$$

Once the total number of moles stored is collected through the volumetric experiment, a correction is applied for the sorbed phase and rock pore volume compressibility effects. To account for the pore compressibility, the new sample pore volume available for storage at the end of a pressure step changes from V_{si} to V_{sf}.

$$V_{si} = V_{p0}\left(1 + C_p P_i\right) \quad \text{.....(17)}$$

$$V_{sf} = V_{p0}(1 + C_p P_f) \quad \text{.....(18)}$$

Therefore, by substituting V_{si} and V_{sf} into **Eq. 16**, the number of moles stored is expressed in terms of pressure, volume, and pore compressibility C_p.

$$\frac{P_i}{z_{P_i}}\left\{V_{p0}\left(1 + C_p P_i\right)\right\} - \frac{P_f}{z_{P_f}}\left\{V_{p0}\left(1 + C_p P_f\right)\right\} = \frac{P_{rf} V_r}{z_{rf}} - \frac{P_{ri} V_r}{z_{ri}} + \frac{P_{df} V_d}{z_{df}} - \frac{P_{di} V_d}{z_{di}} \quad \text{.....(19)}$$

To calculate the pore compressibility, two equations with two unknowns (pore compressibility C_p and pore volume at reference pressure V_{p0}) are utilized over two pressure steps. while the presence of sorption is ignored.

$$C_p = \frac{\frac{V_r\left(\frac{P_{f1}}{z_{f1}}-\frac{P_{ri1}}{z_{ri1}}\right)+V_d\left(\frac{P_{f1}}{z_{f1}}-\frac{P_{di1}}{z_{di1}}\right)}{V_{p0}}+\frac{P_{f1}}{z_{f1}}-\frac{P_{pi1}}{z_{P_pi1}}}{\frac{P_{pi2}^2}{z_{P_pi2}}-\frac{P_{f2}^2}{z_{f2}}} \quad \text{.....(20)}$$

Once pore compressibility (C_p) and pore volume at reference pressure (V_{p0}) are obtained using **Eq. 19** and **Eq. 20**, the effective pore volume is predicted using:

$$V_{\text{eff}} = \left[V_{p0}\left(1 + C_p P_f\right)\right] \quad \text{.....(21)}$$

4.2 Estimation of Sorbed Gas Storage Parameters using CO_2

Next step of the experiment includes the estimation of the Langmuir parameters, namely G_{sL} and P_L, related to the CO_2 sorption by the sample. Santos and Akkutlu (2013) proposed estimating the Langmuir parameters by using a linearized form of the Langmuir model.

Notice that **Eq. 22** in its linear form gives a straight line when the laboratory data is plotted as $(1/n_{s,s,i})$ versus $1/P_{f,i}$. In turn, the Langmuir parameters can be obtained with certainty from the slope and intercept where $n_{s,s\,i}$ is the number of moles stored in sorbed phase at final pressure P_f at stage i.

$$\frac{1}{n_{s,s\,i}} = \frac{1}{n_{s,smax}} + \left(\frac{P_L}{n_{s,smax}}\right)\frac{1}{P_{f,i}} \quad \text{.....(22)}$$

At least two stages of measurements are recommended to identify the linearity. Once the parameters are obtained, the isotherm can be constructed. Note that the maximum sorption capacity

can be converted from moles to scf/ton using **Eq. 23** $G_s = n_{s,s}\mathrm{M}/(w\rho_{s,s})$ where ρ_s is 1.87 x 10^{-3} g/cc and 6.76 x 10^{-4} g/cc for CO_2 and CH_4 accordingly at standard conditions. The final parameter, representing the maximum density of the adsorbed phase when CO_2 is stored at the maximum capacity ($\rho_{s,s\,max}$), is often predicted independently using molecular pore models and applying equilibrium molecular dynamics simulation.

$$G_s = n_{s,s}M/(w\rho_{s,s}) \quad \text{.....(23)}$$

The stored sorbed gas volume corrected for the pore compressibility and sorbed phase effects ($n_{s,s\,i}$) is given in **Eq. 24**:

$$n_{s,s,i} = \frac{n_{s,\mathrm{tot,i}} - \frac{P_{fi}}{z_f RT}[V_{p0}(1+C_p P_{fi})]}{1 - \frac{P_{f,i}}{z_f RT}\left(\frac{1}{\rho_{s,s\,max}}\right)} \quad \text{..... (24)}$$

The $\boldsymbol{n_{s,\mathrm{tot,i}}}$ in the numerator of **Eq. 24** is the sorbed amount measured using the mass balance at the equilibrium pressure $\boldsymbol{P_{f,i}}$ at the stage *i*. This amount has not been corrected yet for the pore compressibility and sorbed phase effect; the term $\boldsymbol{P_f\left[V_{p0}\left(1 + C_p P_f\right)\right]/(z_f RT)}$ in **Eq. 24** accounts for the pore compressibility effect and $\boldsymbol{P_f/(z_f \rho_{s,max} RT)}$ in the denominator of **Eq. 24** accounts for the sorbed phase effects. Here, $\boldsymbol{n_{s,s\,i}}$ is the corrected sorbed amount ready for the straight-line analysis. I recommend at least three stages of gas expansion for completion of Step 2. In this paper, the results include five stages. Once all parameters are known, sorbed gas is calculated by applying the Langmuir model.

4.3 Estimation of Compressed Free Gas and Sorbed Gas Storage

The free gas amount estimated from (**Eq. 25**) for sequestering CO_2 at final (or "target") pressure P_f using:

$$n_{s,\mathrm{free}} = \frac{P_f V_{\mathrm{eff}}}{z_f RT} \quad \text{..... (25)}$$

Here, $n_{s,\text{free}}$ is the number of moles of free gas stored in the sample. This value can be converted into G_f in SCF/ton using density of target gas in free-phase at standard conditions (ρ_{free}).

$$G_f = n_{s,free} M/(w\rho_{s,free}) \quad \text{.....(26)}$$

To calculate the effective pore volume $V_{eff\,1}$ at various pressures, changes due to the presence of the adsorbed phase which underestimate current void space, in addition to pore rock compressibility, is accounted for by an adsorption factor (**Eq. 27**). This value is then used to calculate the amount of free gas stored in the sample as effective stress changes. The change in the adsorbed volume ΔV_{ads} is calculated using the Langmuir model in terms of cm^3.

$$V_{eff\,1} = V_{p0} + \Delta V_{cp} - \Delta V_{ads} \quad \text{.....(27)}$$

where:

$$\Delta V_{Cp} = C_p V_{p0} P$$

$$\Delta V_{ads} = V_{ads,(i+1)} - V_{ads,i}$$

Sorbed gas storage can then be calculated at any pressure by Eq. 6.

4.4 Estimation of Total Gas Storage

The total amount of moles stored in a sample can be separated into free ($n_{s,free}$ or G_f) and sorbed ($n_{s,s}$ or G_s) volumes. It can also be written as the sum of the Langmuir isotherm and the free gas equation of state to account for both storage methods respectively (**Eq. 28**).

$$n_{s,tot} = n_{s,s} + n_{s,free} = n_{s,s\,\max} \frac{P_f}{P_f + P_L} + \frac{P_f}{z_f RT}(V_{eff}) \quad \text{.....(28)}$$

or in terms of scf/ton $G_t = G_s + G_f$

Table 4 — Key storage-related parameters of the samples obtained using Helium gas expansion.

Helium						
Sample	Core Length (mm)	Core Diameter (mm)	Core Dry Weight (g)	TOC (%)	Reference Pore Volume (cc)	Pore Compressibility (psi^{-1})
21	45.44	25.21	59.07	3.90	0.42	5.42E-06
23	24.61	25.02	30.17	4.00	0.65	7.05E-06
25	24.21	25.3	30.04	3.70	0.72	1.75E-05
26	24.89	25.28	30.64	4.95	0.88	2.77E-06
27	25.73	25.3	31.56	4.74	0.80	1.13E-05
39	20.65	24.86	26.02	1.80	0.69	5.17E-05
Average	27.59	25.16	34.58	3.85	0.69	1.60E-05

4.5 Shale Samples Properties

In this study, the proposed procedure is implemented to six source rock samples. Five samples were taken from Barnett shale and another sample from another source rock. The samples and their TOC are tabulated in **Table 4** in which their values range in 1.8-5.0 %.

4.6 Estimate CO_2 in Place for Individual Shale Gas Plays using Laboratory Measurements

The total storage capacity of a shale gas play can be estimated by applying the previous methodology to samples of different plays at initial reservoir conditions, namely pressure. More specifically, the volume for each storage mechanism can be calculated using parameters obtained in the laboratory and the areal extent of the formation. A formation's storability can be further divided by developed area, undeveloped area, and total (developed+undeveloped) area.

Sequestration volumes in terms of scf/ton are converted to scf by assuming a rock density of 2.63 g/cc.

5 RESULTS AND DISCUSSION

5.1 Results of Free Gas Storage Parameters using Helium

The key parameters of reference pore volume V_{p0} and pore volume compressibility C_p are predicted using the Helium gas expansion method. Clearly, the samples have low pore volume estimated with values changing in between 0.42-0.88 cc with an average pore volume of 0.66 cc. Note that, as mentioned in the previous section, these pore volume values could change due to pore compressibility and sorption effects with changing pressure. The predicted pore compressibility values were in between $2.8\text{x}10^{-6}$-$1.7\text{x}10^{-5}$ 1/psi. Similar values were obtained by Kang et al. (2011) and Aldana et al. (2021). **Fig. 9** shows the effective pore volume V_{eff} predicted as a function of pressure for the samples.

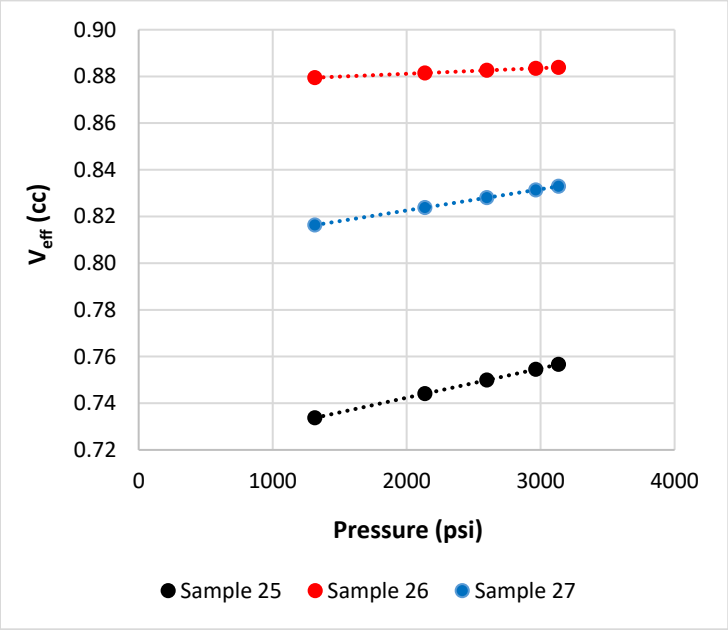

Figure 9 — Effective volume V_{eff} of three Barnett shale samples are shown as a function of pore pressure. The data points are obtained using the Step 1 of the procedure.

5.2 Results of Sorbed Gas Storage Parameters using CO_2 and CH_4

The values Langmuir volume and Langmuir pressure for CO_2 and CH_4 gases are tabulated on **Table 5**. Although most of them were acquired experimentally, the Langmuir parameters for Sample 39 were obtained from Santos (2012). The Langmuir pressures and volumes are of the same order of magnitude. On average, Langmuir pressure is larger for both CO_2 gas and CH_4 gas

Table 5 — Langmuir parameters of the samples obtained for CO_2 and CH_4 gas.

	CO_2		CH_4	
Sample Number	Langmuir Pressure (psi)	Langmuir Volume (scf/ton)	Langmuir Pressure (psi)	Langmuir Volume (scf/ton)
21	2,803.0	1,428.6	3,270.9	52.9
23	5,197.5	5,000.0	-	-
25	3,420.9	1,250.0	-	-
26	2,963.0	1,000.0	-	-
27	3,201.9	1,250.0	3,672.6	109.9
Average	3,517.3	1,985.7	2,544.5	81.4

Also shown on **Fig. 10** is the Langmuir isotherm constructed from the parameters obtained via its linear form using CO_2 as the measuring fluid. Each sample has its own set of Langmuir parameters. Hence, one $1/G_s$ vs $1/P$ plot per sample was constructed with a minimum of two data points as that is all that is needed to obtain the Langmuir isotherm.

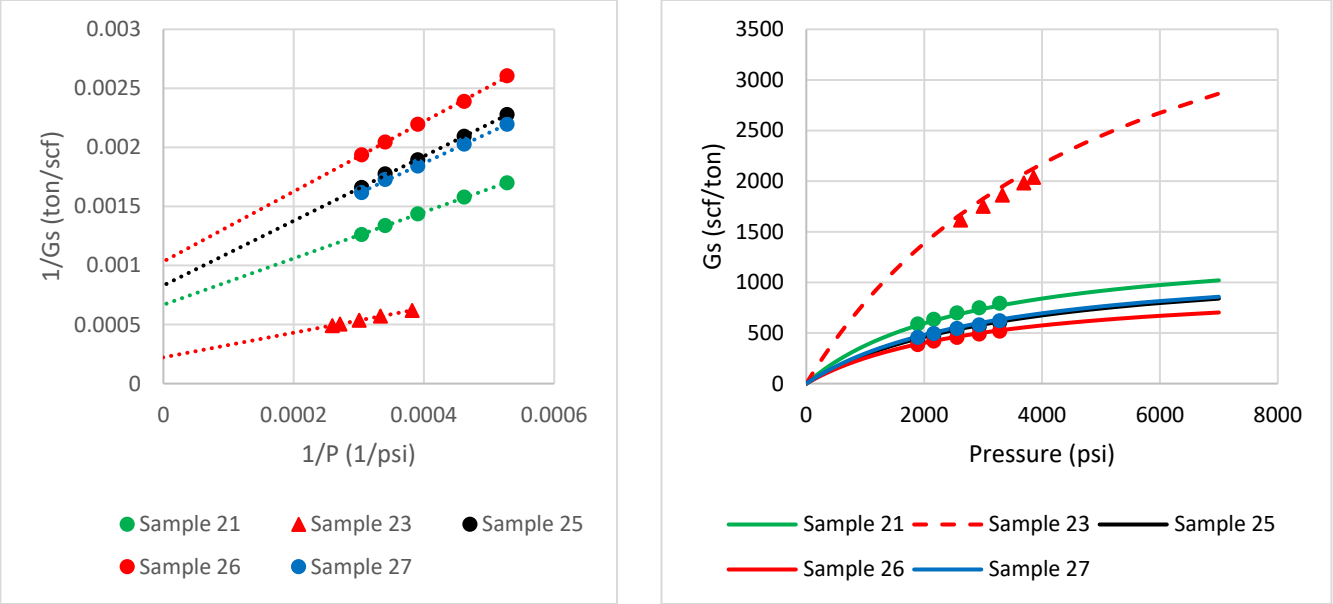

Figure 10 — (Left) Linear form of Langmuir model obtained through laboratory experiments, and (Right) the Langmuir model constructed after the Langmuir Pressure ($\boldsymbol{P_L}$) and Maximum Sorption Capacity ($\boldsymbol{G_{sL}}$) values were obtained for the samples analyzed through its linear form.

The key parameters of Langmuir volume and Langmuir pressure were obtained by plotting $1/G_s$ vs $1/P$, where $1/G_{sL}$ is the y-intercept and the slope is P_L/G_{sL} per **Eq. 29** (the scf/ton equivalent of **Eq. 22**) , in the linear form of the Langmuir model. Here, the sorption capacity is represented by G_{sL}, which is found by the inverse of the intercept. Once G_{sL} is known, the Langmuir pressure is determined from the slope. The intercept for Sample 21 is 0.0007 ton/scf, such that G_{sL} equals 1428.6 scf/ton. Therefore, according to their CO_2 gas Langmuir volumes, the samples that have the largest sorbed storage capacity are Samples 23, 21, 27, 25, and 26 in increasing order. The Langmuir pressure for Sample 21 equals 2,803 psi. The Langmuir model plots using CO_2 and CH_4 for Samples 23, 25, 26, 27, and 39 are further discussed next.

$$\frac{1}{G_s} = \frac{1}{G_{sL}} + \left(\frac{P_L}{G_{sL}}\right)\frac{1}{P} \quad \text{.....(29)}$$

5.3 Results of CO_2 Storage Values

The maximum sorbed phase density ($\rho_{s,s\,max}$) values of 1.18 g/cc and 0.34 g/cc were used for CO_2 and CH_4, respectively (Span and Wanger 1996, Ambrose et al. 2012).

The total, free, and sorbed gas volumes for each sample were calculated using the measured Langmuir volume and pressure up to approximately 3,200 psi shown in **Table 6** and **Table 7**. The maximum amount of CO_2 sorbed per sample ranged from 515 to 2040 scf/ton, with an average of 915 scf/ton. However, free gas stored the values ranged from 80 to 460 scf/ton with an average 340 scf/ton. Comparing the overall amount of gas stored per measurement gas, the maximum total amount of CO_2 stored per sample ranged from 875 to 2400 scf/ton, with an average of 1260 scf/ton.

Table 6 — Sample 21, 23, 25, 26 and 27 sorbed, free, and total CO_2 gas volumes.

CO_2			
Sample	Adsorption (scf/ton)	Free (scf/ton)	Total (scf/ton)
21	792.5	83.1	875.6
23	2,038.1	358.6	2,396.7
25	602.7	400.4	1,003.1
26	516.4	457.3	973.7
27	618.8	419.1	1,037.9
Average	913.7	343.7	1,257.4

Table 7 — Sample 21, 23, 25, 26 and 27 sorbed to free-phase CO_2 gas ratio.

CO_2	
Sample	Sorbed to Free-Phase Ratio
21	9.5
23	5.7
25	1.5
26	1.1
27	1.5

The dominant storage contribution varied by sample for CO_2 gas. For Samples 21 and 23 (**Fig. 10**), adsorption was the primary storage mechanism with adsorption volumes being five times larger than free-phase storage volumes at approximately 3,000 psi, the maximum pressure applied. In general, storage volume increased with pressure. Sample 26 (**Fig. 11)** indicated a 2:1 ratio of sorbed gas to free-phase gas. Similarly, Samples 26 and 27 (**Fig. 11, Fig. 12**) there was a 1:1 ratio of sorbed to free-phase gas stored., while for Sample 27, most of the gas was stored as compressed free gas. The maximum pressure applied in the laboratory was ~3200 psi, however, the models were extrapolated further to show the trend behavior of the different storage components.

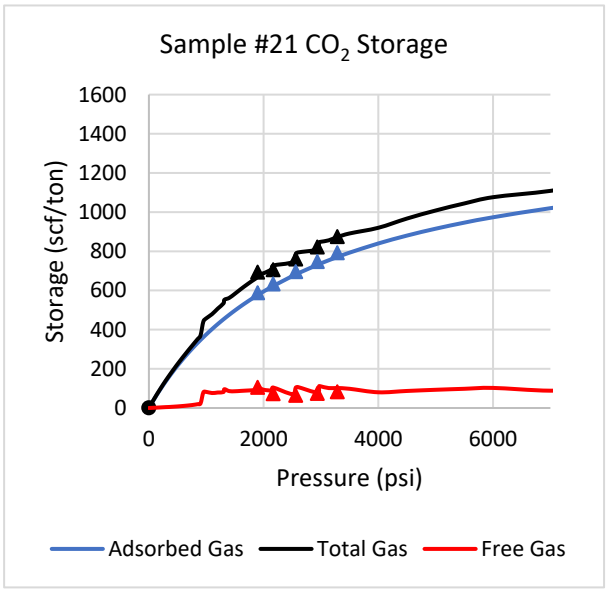

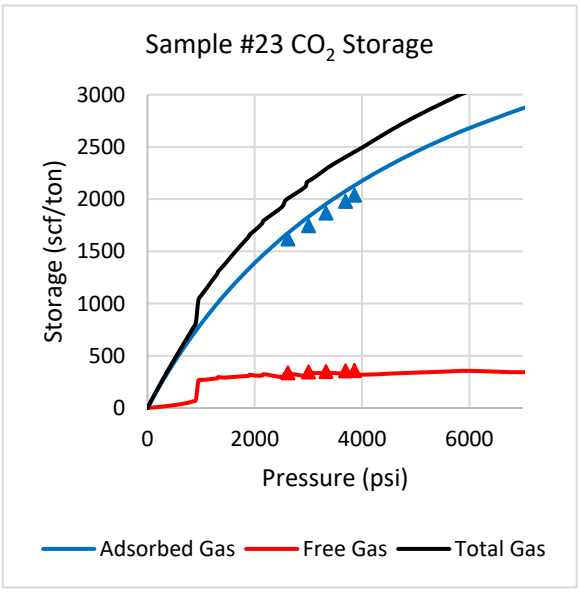

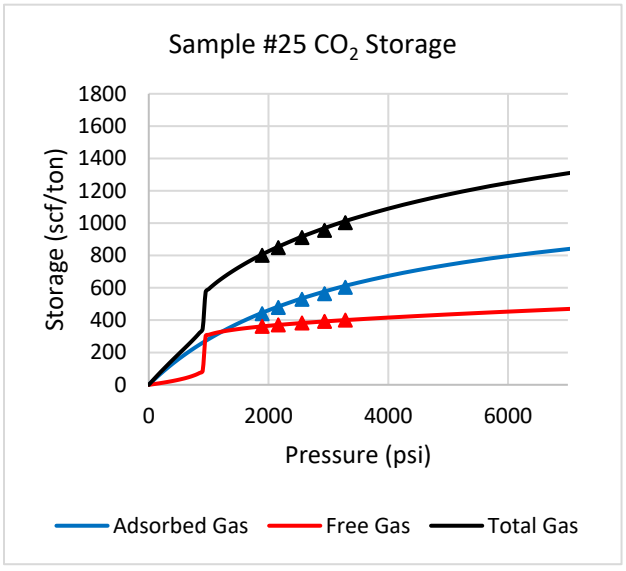

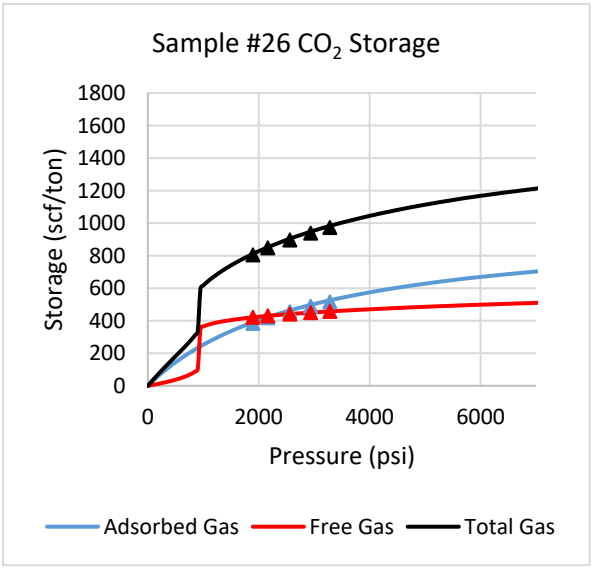

Figure 11 — CO_2 total, sorbed, and free-phase storage measurements for Samples 21, 23, 25, 27.

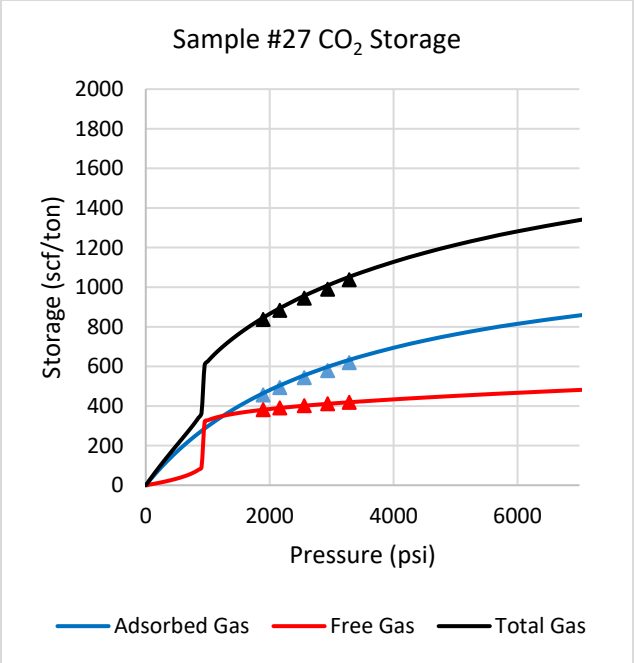

Figure 12 — CO_2 total, sorbed, and free-phase storage measurements for Samples 25, 26, 27.

5.4 Results of CH_4 Storage Values

The maximum amount of methane sorbed per sample ranged from 35 to 50 scf/ton, with an average of 43 scf/ton, while for free gas stored the values ranged from 55 to 210 scf/ton with an average 130 scf/ton (**Table 8**). Ultimately, the maximum total amount of methane stored per sample ranged from 90 to 260 scf/ton, with an average of 70 scf/ton. Thus, free-phase storage was the dominant storage method for CH_4 gas (**Fig. 13**) exhibited by Sample 21 and Sample 27 with a 2:1 and 4:1 free-phase to sorbed gas ratio respectively (**Table 9**). Sample 39 provided similar sorbed values of approximately 100 scf/ton at 3,000 psi (**Fig. 14**). In this procedure, the pore volume was assumed constant. However, as shown previously, the effective pore volume changes with increasing stress. This behavior causes the sorbed gas volume correction to sorption to trend positively instead of negatively, yielding unreasonable results of negative storage. Samples 23,

25, and 26 showed this behavior, therefore their final values were omitted. This observation is supported by Santos and Akkutlu (2013).

Table 8— Samples 21 and 27 sorbed, free, and total CH_4 gas volumes.

CH_4			
Sample	Adsorption (scf/ton)	Free (scf/ton)	Total (scf/ton)
21	35.6	56.9	92.5
27	50.7	207.7	258.4
Average	43.2	132.3	175.5

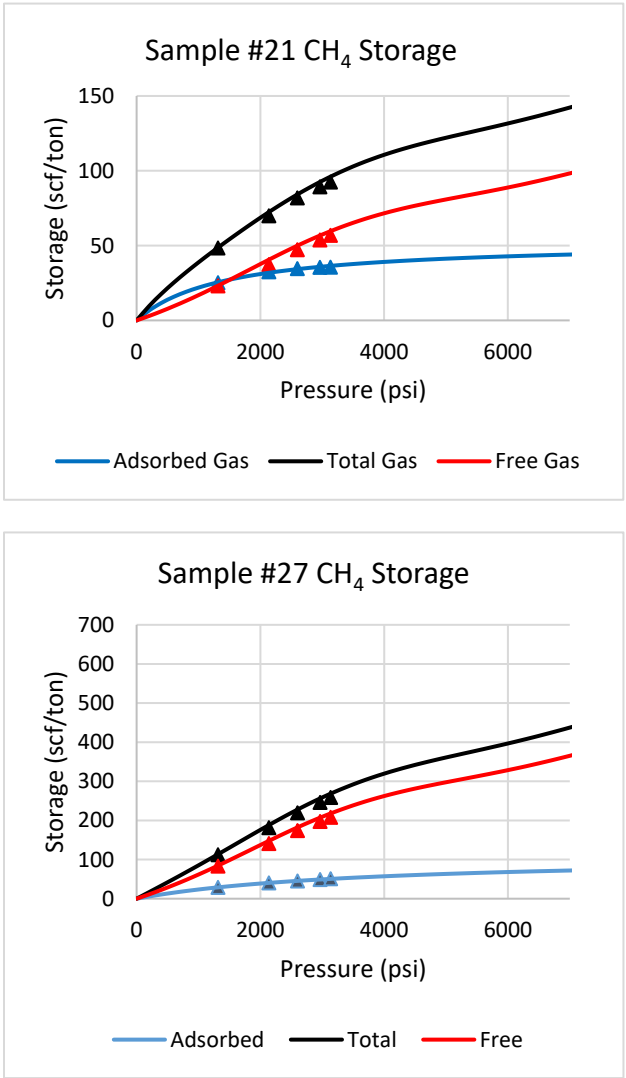

Figure 13 — CH_4 total, sorbed, and free-phase storage measurements for Samples 21 (top) and 27 (bottom).

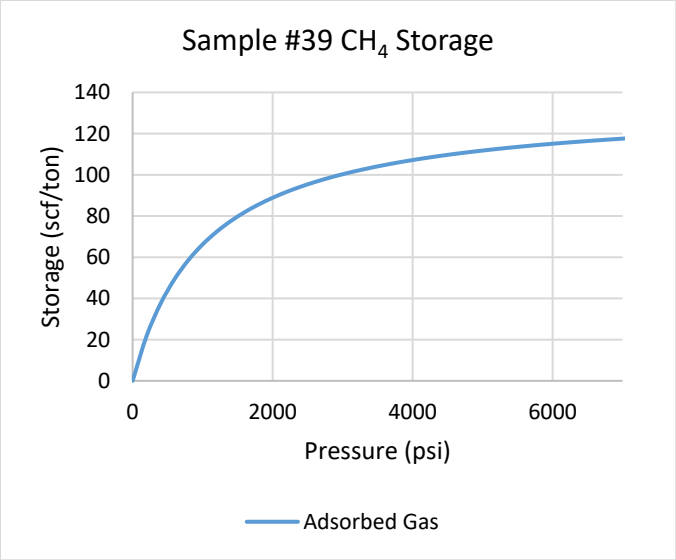

Figure 14 — CH_4 sorbed phase storage measurements for Sample 39.

Table 9 — Samples 21 and 27 free-phase to sorbed CH_4 gas ratio.

CH_4	
Sample	Free-Phase to Sorbed Gas Ratio
21	1.6
27	4.1

5.5 CH_4 Compressed Free Gas Component Anomaly

The sorbed gas models constructed all roughly follow the Langmuir isotherm trend, while for CH_4, the free gas storage steadily increases over pressure until about 4,000 psi where it levels out. Around 5,000 psi, it continues to increase but at a slightly lower rate and in a linear fashion. The change in trend occurs once the sorption capacity of the rock has leveled and maximum sorption capacity appears to have been reached. Therefore, it is concluded that once the available pores surface area has been filled, the free-phase gas starts to fill the remaining vacant middle portion of the pore. Once full, the volume of free-phase gas is further squeezed into the pore and

increases with increasing pressure. Perhaps the reason that the trend is linear at higher pressure as opposed to lower pressure is because there is no competing storage mechanism occurring simultaneously, since sorption capacity has been exhausted. As the free-phase storage dominates, its signature is also reflected in the total stored gas trend.

5.6 Comparison of CH_4 and CO_2 Sorbed Gas Storage Results

The total and sorbed gas stored were compared on **Fig. 15**. The storage volumes for CO_2 gas were greater than CH_4 for both mechanisms. For Samples 21 and 27, samples stored at least three times more sorbed CO_2 gas. Overall, the uptake of CO_2 is larger than that of CH_4 for sll three storage components (total, free, sorbed). Two factors contribute to this phenomenon. First, CO_2 steric effects and its affinity to shale facilitates molecular interaction of the rock and gas molecule which enhances the adsorption of CO_2. Second, the linearity of the CO_2 molecular structure enables further access into the smaller pores of the organic matrix. Since the organic pores are the main storage site for adsorption, accessibility into them is crucial, thus the linearity of the CO_2 molecular structure is advantageous. This process is called molecular sieving shown in **Fig 16** (Kang et al, 2011). It has been discussed that CO_2 has the capacity to displace CH_4 by competitive sorption, and this concept can be applied to improved oil recovery (IOR) of gas reservoirs (Huo et al. 2017). In this study, the storage experiments were performed with pure gases, however, Du et al. 2020 and Qi et al. 2018 considered a mixture of CO_2 and CH_4. Their findings agree with the results presented. Similarly, they observe an increase in CO_2 adsorption as the CO_2 content of the mixture increases

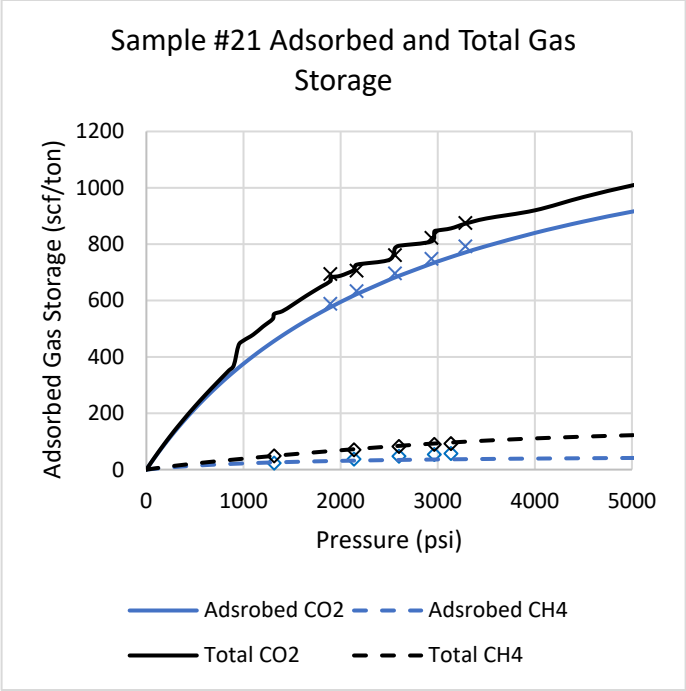

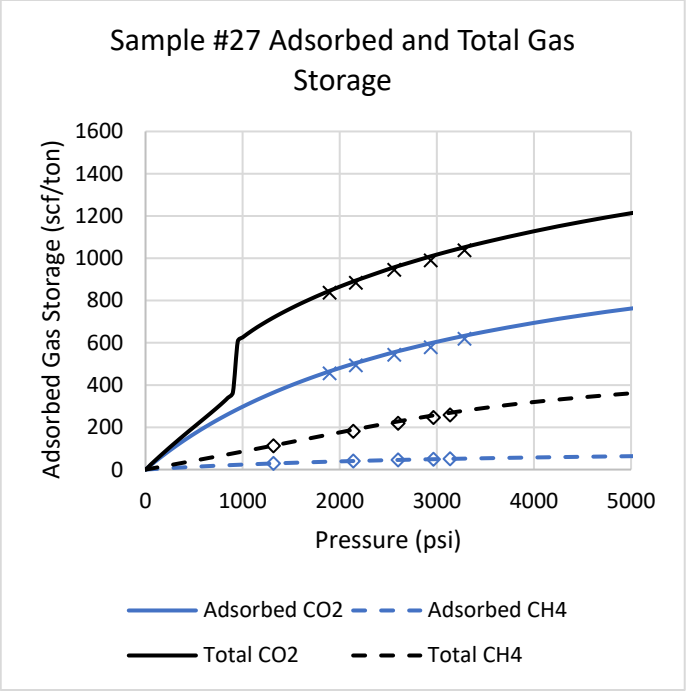

Figure 15— CO_2 and CH_4 total and sorbed storage measurements of total and sorbed gas for Sample 21 and Sample 27.

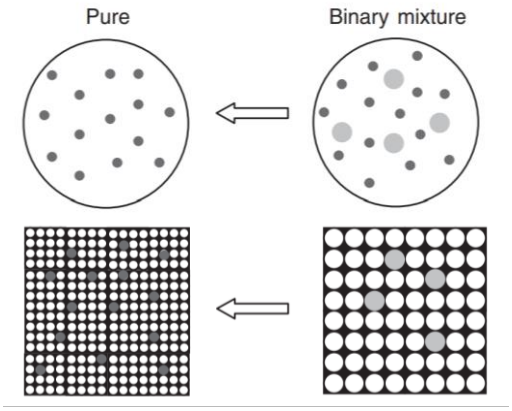

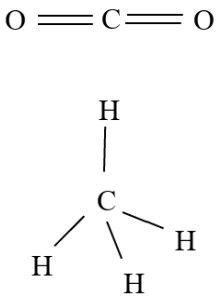

Figure 16 — (Left) Schematic of molecular sieving in kerogen where the larger molecule represents CH_4 and the smaller molecule represents CO_2 accordingly reprinted from Kang et al. (2011) and (Right) the molecular structure of CO_2 is linear while of CH_4 is tetrahedral.

5.7 Considerations of Sorption and Pore Compressibility Effects

The adsorption and pore compressibility effects correction are relevant because these can decrease the pore volume available for sequestration. These considerations allow for higher accuracy in storage capacity evaluation in organic rich-shale rock. Applying them to samples under confining reservoir pressure allows for a more representative sequestration estimation. This undertaking can be beneficial not only for CCUS purposes, but also for improved oil recovery.

6 ESTIMATION OF CARBON SEQUESTRATION POTENTIAL OF EXISTING SOURCE ROCKS IN NORTH AMERICA

With the present methodology, entire gas shale play storage capacity can be estimated. This estimate is different than the one I showed in Chapter 1. The total storage computed now considers both sorption and free gas storage. In addition to the Barnett shale, the Marcellus, Fayetteville, Eagle Ford, and Haynesville shales in North America were considered. I chose only shale gas reservoirs as the potential locations for the sequestration as I carefully explained it in the introduction as ideal alternative locations for carbon sequestration. For some plays, the developed and undeveloped areas are known, therefore their storage potential were calculated accordingly. Overall, total storage over total area was estimated for all shales.

Table 10 — North American Shale Gas Play Characteristics.

	Barnett	**Marcellus**	**Fayetteville**	**Eagle Ford**	**Haynesville**
Initial Pressure (psi)	3,000	3,500	2,000	5,000	10,000
Total Acreage (sq. mi)	14,300	82,000	4,300	200	9,000
Average Formation Thickness (ft)	300	125	200	200	250
Average Developed Area (sq. mi)	8,000	42,600	2,700	-	2,700
Average Undeveloped Area (sq. mi)	6,300	39,400	1,600	-	1,600
Average Initial Temperature (°F)	190	135	175	-	315

6.1 Calculated Initial CO_2 Sequestration Capacity at Initial Reservoir Conditions

Using this simple estimation, the following free gas CO_2 storage capacity at initial reservoir conditions is estimated for the Barnett shale using the parameters in **Table 10**. The CO_2 volume that can be stored at the Barnett shale initial reservoir conditions is calculated using the inverse relationship between stored gas (G) and the formation volume factor (B_{gi}). First, the B_{gi,CH_4} and B_{gi,CO_2} are calculated. Then, they are imputed into **Eq. 3**.

$$G_{CO_2} = G_{CH_4}\left(\frac{B_{gi,CH_4}}{B_{gi,CO_2}}\right) = 508\ Tcf\ \left(\frac{5.093x10^{-3}}{2.449x10^{-3}}\right) = 1057\ Tscf \quad \text{.....(32)}$$

The calculated free gas value of possible CO_2 storage value at initial reservoir conditions is 1056 Tscf in the Barnett shale.

6.2 Storage Potential in Developed Area

6.2.1 Free Gas Estimation with Pore Compressibility Adjustments

The compressed gas storage component is calculated using **Eq. 27** at average initial reservoir pressure. For this, $V_{\text{eff }1}$ must be calculated first from laboratory measured parameters. For this example, Sample 21 was used.

Where $V_{\text{eff }1} = \text{V}_{\text{p0}} + \Delta V_{Cp} - \Delta V_{ads}$ and Langmuir volume is in cm^3:

$$V_{\text{eff }1} = 0.42\ cc + (\ 5.42x10^{-6}\ psi^{-1}\ x\ 0.42\ cc\ x\ 3000\ psi) - \left(4.28\ cc\frac{3000\ psi}{3000+2803\ psi} - 4.28cc\frac{2964\ psi}{2964+2803\ psi}\right) \quad \text{.....(33)}$$

$$V_{\text{eff }1} = 0.41\ cm^3$$

Once $V_{\text{eff }1}$ is known, input its value into **Eq. 25**:

$$n_{s,free} = \frac{P_f V_{\text{eff }1}}{z_f RT} = \frac{3000\ psi\ x\ 0.41\ mol}{0.401\ x\ 1206.4\ psi\ cm^3\ K^1\ mol\ x\ 298.15\ K} = 8.5x10^{-3}\ \text{mol} \quad \text{.....(34)}$$

The free gas stored volume is then converted from moles to scf/ton using $G_f = n_{s,free}\text{M}/(\rho_{s,free}\, w)$ and density of target free gas (eg. CO_2) at standard conditions:

$$G_f = \frac{8.5x10^{-3}\ \text{mol x}\ 44.01\frac{\text{g}}{\text{mol}}}{0.00187\frac{g}{cm^3} x\ 6.511\ x1o^{-5}\ ton} = 3.07x10^6\ \frac{cc}{ton} = 317.7\ \frac{cc}{ton}\ x\frac{3.531x10^{-5}}{1}\frac{ft^3}{cc}\ = 108.5scf/ton$$

…….(35)

Assuming a rock density of 2.63 g/cc, a new storage capacity in units of scf/acre is calculated.

$$G_f = G_f\ \frac{scf}{ton} x\ \rho_{shale}\frac{g}{cc}\ x\frac{1}{32}\frac{\frac{ton}{scf}}{\frac{g}{cc}}\ xAverage\ formation\ thickness\ ft\ x\ \frac{1}{0.000023\frac{acre}{ft^2}}$$……(36)

$$G_f = 108.5\frac{scf}{ton}\ x\ \frac{1}{32}\frac{\frac{ton}{scf}}{\frac{g}{cc}}2.63\frac{g}{cc}\ x\ 300\ ft$$

$$x\ \frac{1}{0.000023\frac{acre}{ft^2}} = 116.8\ \text{MMscf/acre}$$……..(37)

The storage possible in a developed area considers only the average area that has already been produced. Thus, an average developed area of 8000 sq. mi for the Barnett shale is included to convert the storage capacity from scf/acre to scf.

$$G_{f,dev} = G_f\ x\ Average\ developed\ area\ x\frac{1}{0.00156}\frac{acre}{sq\ mi}$$……...(38)

$$G_{f,dev} = 116821097\ x\ 8{,}000\ sq\ mi\ x\frac{1}{0.00156}\frac{acre}{sq\ mi} = 599\ Tscf$$…..……...(39)

6.2.2 Sorbed Gas Estimation

The sorbed gas stored for a developed area is discussed next. Beginning with the Langmuir model, the sorbed storage component at average initial reservoir pressure of the target formation is calculated using the Langmuir parameters obtained experimentally of Sample 21 and **Eq. 6**.

$$G_s = G_{sL}\frac{P}{P+P_L} = 1428.6\frac{3000}{3000+2803} = 739\ scf/ton$$……..……(40)

The storage capacity is first converted to scf/acre, then to scf after using the average developed area of the formation (**Eq. 41**).

$$G_{s,dev} = G_s \; x \; Average \; developed \; area \; x \; \frac{1}{0.00156} \frac{acre}{sq \; mi} \ldots\ldots (41)$$

$$G_{s,dev} = 795675491 \; scf/acre \; x \; 8{,}000 \; sq \; mi \; x \; \frac{1}{0.00156} \frac{acre}{sq \; mi} = 4080 \; Tscf \ldots\ldots (42)$$

The estimated sorbed gas value for the developed area of the Barnett shale is approximately 4080 Tcf.

6.2.3 Total Gas Estimation

To obtain the total storage volume of the developed play, the free gas and sorbed gas storage volumes of the developed area are summed.

$$G_t = G_{f,dev} + G_{s,dev} \ldots\ldots (43)$$

$$G_t = 599 \; Tcf + 4080 \; Tcf = 4679 \; Tscf \ldots\ldots (44)$$

So far, the total gas storage estimation for a developed area indicates the current CO_2 subsurface storage capacity of regions in shale gas plays that have already been produced. Hence, **Table 11** depicts the current storage availability current of the different North American plays.

Table 11 — Gas shale plays calculated CO_2 storage capacity of the developed area.

Developed Average Formation Area			
	Free Gas Storage Capacity (Tscf)	Sorbed Gas Storage Capacity (Tscf)	Total Gas Storage Capacity (Tscf)
Barnett	605	4,057	4,662
Marcellus	1,194	9,668	10,862
Fayetteville	115	735	850
Haynesville	303	2,988	3,291
Total	2,217	17,447	19,664

6.3 Storage Potential in Undeveloped Area

The storage capacity in undeveloped areas of a formation indicate its potential for carbon sequestration in the future once it has been produced for methane. The calculations for the previous section are then performed using the average undeveloped area for the chosen shale gas formations. The results are shown in **Table 12**.

Table 12 — Gas shale plays calculated CO_2 storage capacity of the undeveloped area.

Undeveloped Average Formation Area			
	Free Gas Storage Capacity (Tscf)	Sorbed Gas Storage Capacity (Tscf)	Total Gas Storage Capacity (Tscf)
Barnett	477	3,195	3,672
Marcellus	1,104	8,941	10,045
Fayetteville	68	436	504
Haynesville	280	2,758	3,038
Total	1,929	15,329	17,258

Table 13 — Gas shale plays calculated CO_2 storage capacity of the total (developed + undeveloped) area.

Total Average Formation Area			
	Free Gas Storage Capacity (Tscf)	Sorbed Gas Storage Capacity (Tscf)	Total Gas Storage Capacity (Tscf)
Barnett	1,082	7,251	8,333
Marcellus	2,298	18,609	20,907
Fayetteville	184	1,171	1,355
Eagle Ford	9	84	93
Haynesville	582	5,746	6,328
Total	4,155	32,860	37,015

6.4 Total Storage Potential

The total storage potential for the plays presented are in the trillion standard cubic feet range. Barnett shale has the potential to store 8,300 Tscf in its entirety and the Marcellus could theoretically sequester 21,000 Tscf as well (**Table 13).** In contrast, the Eagle Ford, Fayetteville, and Haynesville have less storage potential. With these 5 sites, there is a total storage

6.5 Discussion of Known and Calculated Storage Volumes

Two calculated CO_2 storage volumes have been calculated:

1) Free gas volume using G and B_{gi} inverse relationship from Svetlana et al. (2018) based on the initial free gas methane volumes (**Eq. 3**).
2) Free and sorbed gas volume using laboratory obtained parameters using Sample 21.

Here I assume the Marcellus, Fayetteville, Eagle Ford and Haynesville shale gas plays exhibit a similar storage behavior as the one observed in the laboratory from Sample 21. Sample 21 showed a sorbed to free CO_2 gas ratio of 9.5:1 (**Table 7**). This behavior is reflected in the calculated total storage

Table 14 —Total CO_2 storage volume comparison chart adapted from Svetlana et al. (2018).

CO_2 volume calculation Method	Barnett	Marcellus	Fayetteville	Eagle Ford	Haynesville	Total
Inverse G and B_{gi} relationship using free gas methane volumes from Svetlana et al. (2018) (Tscf)	1057	3400	219	-	904	5,580
Inverse G and B_{gi} relationship using free gas methane volumes from Svetlana et al. (2018) (**Megaton**)	55,128	177,399	11,439	-	47,165	291,131

Table 14 — Continued.

CO_2 volume calculation Method	Barnett	Marcellus	Fayetteville	Eagle Ford	Haynesville	Total
Laboratory method (Tscf)	8,333	20,907	1,354	92	364	36,923
Laboratory method (**Megaton**)	434,760	1,090,786	70,662	4,800	330,163	1,926,376

volumes using the laboratory methods versus the volumes estimated by Svetlana et al. (2018) in which only free gas was considered. To meet the target estimated by the IEA (2021b) to limit global temperature increase to 2°C by 2050, 44,800 Mt of CO_2 must be sequestered to reach net-zero assuming yearly emissions decrease until 2050. However, if emissions remain constant, then 693,000 Mt must be stored to reach net-zero

Using the density of CO_2 at standard conditions of 0.116868 lb/ft^3, the storage values from this study were converted from Tscf to Mega-ton (**Table 14**). In these 5 formations, according to laboratory measurements, there is abundant storage capacity to reach the IEA (2021b) climate target. The Marcellus holds the biggest potential with an optimistic 20,907 Tscf or 1,090,786 Mt of storage followed by the Barnett with 434,760 Mt. The Eagle Ford had the least potential 4,800 Mt due to the relatively small area of the formation followed by the Fayetteville with 70,643 Mt of storage capacity due to its thin formation thickness. Fayetteville shale alone has the potential to sequester 70,662 Mt of CO_2, while only an optimistic 44,800 Mt is required to limit the earth's temperature from rising by 2°C by 2050 considering emission reduction efforts succeed. Alternatively, assuming emissions remain constant over time, both the Barnett and Haynesville must be considered at their full storage potential or approximately 60% of the Marcellus must be used.

5. CONCLUSION

CO_2 storage capacity of organic-rich shale source rocks was measured in the laboratory using six samples. The Santos and Akkutlu model (2013) was employed which involved performing experiments using the volumetric method and a Hassler sleeve holder to apply reservoir equivalent pressures. Corrections were made for adsorption and pore compressibility effects to correct the pore volume available for sequestration with increasing pressure. In addition, a linear form of the Langmuir model was utilized through which the Langmuir volume and Langmuir pressure values were obtained. Other key parameters needed to calculate the total and free gas rock storage capacity were reference pore volume, pore compressibility, and sorbed phase density of which the first two were obtained experimentally, while the latter was assumed from literature. With these, the Langmuir isotherm was constructed and used to measure the adsorptive storability of the rock. Other key parameters needed to calculate the total and free gas rock storage capacity were reference pore volume, pore compressibility, and sorbed phase density of which the first two were obtained experimentally, while the other was assumed from the literature.

Overall, CO_2 possessed the largest stored volume over CH_4, and four of the six samples had the dominant storage method as adsorption. The average CO_2 total, sorbed, and free phase gas stored was 1257.4 scf/ton, 913.7 scf/ton, and 343.7 scf/ton respectively, while for CH_4 it was 175.5 scf/ton, 43.2 scf/ton, 132.3 scf/ton respectively. The higher storage volume for CO_2 can be attributed to the linearity of the CO_2 molecule and its steric effects which enhance access to the minute organic pores and storage in the sorbed phase accordingly. Although a direct relationship between TOC and storage capacity is recognized in the literature, it was not observed here, perhaps due to all samples possessing a similar TOC of ~5%.

Once a storage capacity for a given pressure is obtained, it can be applied to an area of known initial reservoir pressure yielding a storage estimation for an entire formation. The Barnett, Marcellus, Fayetteville, and Haynesville formations have the capacity to individually store more than 44,800 Mt of CO_2, which is the entirety of the conservative atmospheric CO_2 volume needed to prevent catastrophic climatic events due to climate change, if their total (developed+undeveloped) areas are used for sequestration. According to this study, the Marcellus shale can potentially store 1,000,000 Mt of CO_2 gas at full capacity which is more than the estimated storage required to fully sequester current GHG emissions.

It is inevitable that CO_2 emissions will continue to rise due to increase in population and its associated energy demand even with the implementation of renewable energy resources. Thus, carbon capture and sequestration provide a tangible avenue for GHG emission reduction. As the necessity for carbon footprint reduction rises, organic-rich shales can become alternative storage sites as shown by the estimated sequestration capacities of North American plays. Moreover, environmental and petroleum entities can mutually benefit through shared knowledge of enhanced gas recovery and CO_2 sequestration. Although this study focused mostly on the Barnett shale, studies on other organic-rich shale plays with different TOC content should also be further investigated. Lastly, study directly applies a simple and effective storage model (Santos and Akkutlu 2013) that can be easily adopted and employed by the industry.

REFERENCES

Akkutlu, I. Y. and Aldana-Gallego I. 2021 *A New Method for Estimation of Fluid Storage Capacity of Rock Samples and Other Porous Materials under Effective Stress*, US Patent App. 17/332.251 2021.

Aldana-Gallego, I.C., Santos, L.P., and Akkutlu, I.Y. 2021. A Laboratory Method for Estimation of Storage Capacity of Rocks Samples under Effective Stress. ***SPE Journal*** 26(06) 3725-3741. SPE-195552-PA

Ambrose, R. J., Hartman, R.C., Diaz-Campos, M. et al. 2012. Shale Gas in-place Calculations Part I - New Pore-scale Considerations. ***SPE Journal***. 17 (1): 219. SPE-131772-PA.

Azadi, M., Northey, S.A., Ali, S.H. et al. Transparency on greenhouse gas emissions from mining to enable climate change mitigation. *Nature Geoscience.* **13**: 100–104. 2020. Doi: https://doi.org/10.1038/s41561-020-0531-3

Brady, J., Shattuck, D., Parker, M. et al. Video Production Logging and Polymer Gel Yields Successful Water Isolation in the Fayetteville Shale. 2013. Paper presented at the SPE Annual Technical Conference and Exhibition, New Orleans, Louisiana, USA, September 2013. Doi: https://doi.org/10.2118/166301-MS

Brunauer, S., Emmett, P. H., Teller, E. J. Adsorption of gases in multimolecular layers. *Journal of the American Chemical Society*. **60**(2): 309-319. 1938. Doi: https://doi.org/10.1021/ja01269a023

Busch, A., Alles, S., Gensterblum, Y., et al. Carbon dioxide storage potential of shales. *International Journal of Greenhouse Gas Control*, ***2***(3): 297-308. 2008. Doi: https://doi.org/10.1016/j.ijggc.2008.03.003

Charoensuppanimit, P., Mohammad, S. A., and Gasem, K. A. Measurements and modeling of gas adsorption on shales. *Energy & Fuels*, **30**(3): 2309-2319. 2016.

Du, X., Cheng, Y., Liu, Z. et al. 2020. Study on the adsorption of CH4, CO2 and various CH4/CO2 mixture gases on shale. *Alexandria Engineering Journal* **59**(6): 5165-5178. 2020. Doi: https://doi.org/10/1016/j.aej.2020.09.046

Dembicki, H. 2017. Source Rock Evaluation. In *Practical Petroleum Geochemistry for Exploration and Production*, ed. H. Dembicki, Chap. 3, 61-133. Doi: https://doi.org/10.1016/B978-0-12-803350-0.00003-9

Hester, T.C. and Schmoker, J.W. 1985. Selected physical properties of the Bakken Formation, North Dakota and Montana part of the Williston Basin. US Geological Survey, No. **126**.

Gibbs, J.W. The Collected Works of J. W. Gibbs, Longmans and Green: New York, 1928.

Goodman, A., Hakala, A., Bromhal, G. et al. 2011. U.S. DOE methodology for the development of geologic storage potential for carbon dioxide at the national and regional scale.. *International Journal of Greenhouse Gas Control* **5**(4) 952-965. https://doi.org/10.1016/j.ijggc.2011.03.010

Global CCS Institute. 2020. The Global Status of CCS Report 2020. Report. Melbourne, Australia

Gray, I. Reservoir Engineering in Coal Seams: Part 1-The Physical Process of Gas Storage and Movement in Coal Seams. *SPE Res Eng* 2 (01): 28–34. 1987. SPE-12514-PA. Doi: https://doi.org/10.2118/12514-PA

Hammes, U. and Gale, J. 2013. Geology of the Haynesville Gas Shale in East Texas and West Louisiana, U.S.A. In *Introduction*, eds U. Hammes and J.F.W. Gale, 1-4. AAPG Memoir 105.

Hol, S., Peach, C.J. and Spiers, C.J. A new experimental method to determine the CO2 sorption capacity of coal. *Energy Procedia* **4**: 3125-3130. 2011. Doi: https://doi.org/10.1016/j.egypro.2011.02.226

Huo, P., Zhang, D., Yang, Z., Li, W., Zhang, J. and Jia, S., 2017. CO_2 geological sequestration: displacement behavior of shale gas methane by carbon dioxide injection. International Journal of Greenhouse Gas Control, 66, pp.48-59. https://doi.org/10.1016/j.ijggc.2017.09.001

IEA. 2021a. Global Energy Review. CO_2 emissions. Report. IEA, Paris. https://iea.blob.core.windows.net/assets/d0031107-401d-4a2f-a48b-9eed19457335/GlobalEnergyReview2021.pdf

IEA. 2021b. Net Zero by 2050. Report. IEA, Paris. https://iea.blob.core.windows.net/assets/deebef5d-0c34-4539-9d0c-10b13d840027/NetZeroby2050-ARoadmapfortheGlobalEnergySector_CORR.pdf

IPCC. 2001. Farquhar, G.D., Fasham, M.J.R., Goulden, M. et al. The Carbon Cycle and Atmospheric Carbon Dioxide. In: Climate Change 2001: The Scientific Basis. Contribution of Working Group I to the Third Assessment Report of the Intergovernmental Panel on Climate Change. Houghton, J.T., Y. Ding, D.J. Griggs, et al. (eds.). Report. Cambridge University Press, Cambridge, United Kingdom and New York, NY, USA. https://www.ipcc.ch/site/assets/uploads/2018/03/WGI_TAR_full_report.pdf

Ikonnikova, S., Smye, A., Browning, J. et al. Final Report on Update and Enhancement of Shale Gas Outlooks. Bureau of Economic Geology, University of Texas at Austin. 2018. Doi: https://doi.org/10.2171/1479289

Kang S., Fathi, E., Ambrose, R.J., Akkutlu et al. 2011. Carbon Dioxide Storage Capacity of Organic-rich Shales. *SPE Journal*, **16**(4): 842-855. SPE-134583-PA.

Kang, S.M. 2011b. *Carbon Dioxide Storage Capacity of Barnett Shale*. MS Thesis, University of Oklahoma, Norman, Oklahoma (2011).

Kang, S., Shinn, Y., and Akkutlu, I. Y. Gas Storage Capacity of Iljik and Hasandong Shales in Gyongsang Basin, South Korea. Paper presented at the SPE/AAPG/SEG Unconventional Resources Technology Conference, Denver, Colorado, USA, August 2014. Doi: https://doi.org/10.15530/URTEC-2014-1922165

Kim, B. Y., Olorode, O., and Akkutlu, I. Y. Multi-Scale Analysis of CO_2 Injection as Improved Shale Gas Recovery Method. Paper presented at the SPE Europec featured at 81st EAGE Conference and Exhibition, London, England, UK, June 2019. Doi: https://doi.org/10.2118/195528-MS

Krooss, B. V., Van Bergen, F., Gensterblum, Y. et al. High-pressure methane and carbon dioxide adsorption on dry and moisture-equilibrated Pennsylvanian coals. International Journal of Coal Geology, **51**(2): 69-92. 2002. Doi: https://doi.org/10.1016/S0166-5162(02)00078-2

Langmuir, I. Vapor pressures, evaporation, condensation and adsorption. Journal of the American Chemical Society, **54**(7): 2798-2832. 1932. https://doi.org/10.1021/ja01346a022

Li, D., Liu, Q., Weniger, P. et al. High-pressure sorption isotherms and sorption kinetics of CH4 and CO2 on coals. *Fuel* **89**(3): 569-580. 2010. Doi: https://doi.org/10.1016/j.fuel.2009.06.008

Lin, W., Tang, G., and Kovscek, A.R. Sorption-Induced Permeability Change of Coal During Gas-Injection Processes. *SPE Res Eval & Eng* **11**(04): 792–802. 2008. SPE-109855-PA. Doi: https://doi.org/10.2118/109855-PA

Lu, X., Li, F., and Watson, A.T. Adsorption Studies of Natural Gas Storage in Devonian Shales. *SPE Form Eval* **10**(02): 109–113. SPE-26632-PA. 1995. Doi: https://doi.org/10.2118/26632-PA

Male, F., Islam, A.W., Patzek, T.W. et al. 2015. Analysis of gas production from hydraulically fractured wells in the Haynesville Shale using scaling methods. *Journal of Unconventional Oil and Gas Resources*, 10: 11-17. Doi: https://doi.org/10.1016.j.uogr.2015.03.001

Mavor, M.J., Owen, L.B., and Pratt, T.J. Measurement and Evaluation of Coal Sorption Isotherm Data. Paper presented at the SPE Annual Technical Conference and Exhibition, New Orleans, Louisiana, September 1990. SPE-20728-MS. Doi: https://doi.org/10.2118/20728-MS

Nature. 2021. Concrete needs to lose its colossal carbon footprint, https://www.nature.com/articles/d41586-021-02612-5 (accessed 23 November 2021).

Nuttal, B. C., Eble, C., Bustin, R. M., et al. Analysis of Devonian black shales in Kentucky for potential carbon dioxide sequestration and enhanced natural gas production. Report Kentucky Geological Survey/University of Kentucky (DE-FC26-02NT41442). 2005. Doi: https://doi.org/10.1016/B978-008044704-9/50306-2

Ryder Scott Company LP. Bakken downspacing has upside, study shows. 2012. *Reservoir Solutions* **15**(2): 1-8.

Pachauri, R. K. and Meyer, L. A. (eds.). Climate Change 2014: Synthesis Report. Contribution of Working Groups I, II and III to the Fifth Assessment Report of the Intergovernmental Panel on Climate Change. IPCC, Geneva, 2014. https://www.ipcc.ch/site/assets/uploads/2018/05/SYR_AR5_FINAL_full_wcover.pdf

Parker, M. A., Buller, D., Petre, J.E. et al. Haynesville Shale-Petrophysical Evaluation. Paper presented at the SPE Rocky Mountain Petroleum Technology Conference, Denver, Colorado, April 2009. Doi: https://doi.org/10.2118/122937-MS

Patzek, T.W., Male, F., Marder, M. 2013. Gas production in the Barnett Shale obeys a simple scaling theory. *Proceedings of the National Academy of Sciences of the United States of America*, **110**(49), 19731-19736. Doi: https://doi.org/10.1073/pnas.1313380110

Patzek, T.W., Male, F., Marder, M. 2014. A simple model of gas production from hydrofractured horizontal wells in shales. *AAPG Bulletin*, **98**(12): 2507-2529. Doi: 10.1306/03241412125

Qi, R., Ning, Z., Wang, Q., Zeng, Y., Huang, L., Zhang, S. and Du, H., 2018. Sorption of methane, carbon dioxide, and their mixtures on shales from Sichuan Basin, China. *Energy & Fuels*, **32**(3): 2926-2940. Doi: https://doi.org/10.1021/acs.energyfuels.7b03429

Ritchie, H. and Roser, M. 2020. CO_2 and Greenhouse Gas Emissions, https://ourworldindata.org/co2-and-other-greenhouse-gas-emissions (accessed 23 November 2021).

Santos, J.M, and Akkutlu, I.Y. Laboratory Measurement of Sorption Isotherm Under Confining Stress With Pore-Volume Effects. *SPE Journal* 18: 924–931. 2013. SPE-162594-PA. Doi: https://doi.org/10.2118/162595-PA

Santos, J. 2012. *Measurement of Sorption Isotherm Under Confining Stress and Adsorption Layer Effects*. MS Thesis, Texas A&M University, College Station, Texas (2012).

Soeder, D.J. 2008. Resource and Environmental Studies on the Marcellus Shale. Presentation from National Energy Technology. https://mde.maryland.gov/programs/Land/mining/marcellus/Documents/Marcellus_GeoEnv_Soeder.pdf

Siemons, N. and Busch, A. Measurement and interpretation of supercritical CO_2 sorption on various coals. *International Journal of Coal Geology* **69**(4): 229-242. 2007. Doi: https://doi.org/10.1016/j.coal.2006.06.004

Span, R. and Wagner, W. 1996. A new equation of state for carbon dioxide covering the fluid region from the triple-point temperature to 1100 K at pressures up to 800 Mpa. *Journal of physical and chemical reference data* **25**(6): 1509-1596. Doi: https://doi.org/10.1063/1.555991

Svetlana, I., Smye, K., Browning, J. et al. 2018. Final Report Prepared for U.S. Department of Energy: Update and Enhancement of Shale Gas Outlooks. Bureau of Economic Geology. Report, Austin, USA. https://netl.doe.gov/sites/default/files/2020-06/FE0026962-Final-Report.pdf

Tan, J., Weniger, P., Krooss, B. et al. Shale gas potential of the major marine shale formations in the Upper Yangtze Platform, South China, Part II: Methane sorption capacity. *Fuel* **129**: 204-218. 2014. Doi: https://doi.org/10.1016/j.fuel.2014.03.064

Trichel, K., and Fabian, J. Understanding and Managing Bottom Hole Circulating Temperature Behavior in Horizontal HT Wells - A Case Study Based on Haynesville Horizontal Wells. 2011. Paper presented at the SPE/IADC Drilling Conference and Exhibition, Amsterdam, The Netherlands, March 2011. Doi: https://doi.org/10.2118/140332-MS

United Nations. 2019. World Population Prospects 2019. https://population.un.org/wpp/Graphs/Probabilistic/POP/TOT/900 (accessed 23 November 2021).

U.S. Department of Energy, Energy Information Administration. 2011. Review of Emerging Resources: U.S. Shale Gas and Shale Oil Plays. EIA. Report. Washington, D.C., USA. http://www.ourenergypolicy.org/wp-content/uploads/2013/02/usshaleplays-1.pdf.

U.S. Department of Energy and National Energy Technology Laboratory 2009. Modern Shale Gas Development in the United States: A Primer. DOE and NETL. Presentation from Groundwater Protection Council and ALL Consulting. https://netl.doe.gov/sites/default/files/2018-03/Shale_Gas_Primer_2009.pdf

Uzoh, C., Han, J., Hu. L.W. et al. 2010. Economic Optimization Analysis of the Development Process on a Field in the Barnett Shale Formation. The Pennsylvania State University. Report. State College, USA. https://personal.ems.psu.edu/~fkd/courses/egee580/2010/Final%20Reports/Barnett%20Shale.pdf

Wang, F. P., and Reed, R.M. "Pore Networks and Fluid Flow in Gas Shales." Paper presented at the SPE Annual Technical Conference and Exhibition, New Orleans, Louisiana, October 2009. SPE-124253-MS. Doi: https://doi.org/10.2118/124253-MS

Wang, P., Ryberg, M., Yang, Y. et al. Efficiency stagnation in global steel production urges joint supply- and demand-side mitigation efforts. *Nature Communications* **12**: 2066. 2021. Doi: https://doi.org/10.1038/s41467-021-22245-6

Weniger, P., Kalkreuth, W., Busch, A. et al. High-pressure methane and carbon dioxide sorption on coal and shale samples from the Paraná Basin, Brazil. *International Journal of Coal Geology*, **84**(3-4): 190-205. 2010. Doi: https://doi.org/10.1016/j.coal.2010.08.003

Wu, T., Zhao, H., Tesson, S., Firoozabadi, A. 2019. Absolute adsorption of light hydrocarbons and carbon dioxide in shale rock and isolated kerogen. *Fuel* **235**: 855-867. Doi: https://doi.org/10.1016/j.fuel.2018.08.023

Xu, C., Dai, Q., Gaines, L. et al. Future material demand for automotive lithium-based batteries. *Communications Materials* **1**(1): 1-10. 2020. Doi: https://doi.org/10.1038/s43246-020-00095-x

Yusuf, A. 2016. *Integrating stimulation practices with geo-mechanical properties in liquid-rich Plays of Eagle Ford Shale*. PhD dissertation, West Virginia University, Morgantown, West Virginia (2016).

Zahasky, C. and Krevor, S., 2020. Global geologic carbon storage requirements of climate change mitigation scenarios. *Energy & Environmental Science* **13**(6): 1561-1567. Doi: 10.1039/D0EE00674B

Zhang, T., Ellis, G.S., Ruppel, S.C. et al. Effect of organic-matter type and thermal maturity on methane adsorption in shale-gas systems. *Journal of Organic Geochemistry* **47**: 120-131. 2012. Doi: https://doi.org/10.1016/j.orggeochem.2012.03.012